https://doi.org/10.1038/s44328-025-00050-1

Plasmonic biosensors and actuators for integrated point-of-care diagnostics

Han Truong[1,2], Trung Hoang[1], Kyungwha Chung[1,3] ✉ & Luke P. Lee[1,3,4,5,6] ✉

Nanoplasmonic optical antennas function as sensors and actuators, facilitating rapid and selective on-site molecular diagnostics for personalized precision medicine. Here, we highlight advancements in plasmonic biosensors and actuators within point-of-care diagnostics platforms, including optical trapping, cell lysis and ultrafast photonic polymerase chain reaction. Furthermore, we discuss nanoplasmonic optical sensing technologies, and commercial optical diagnostic systems. Nanoplasmonic optical antennas are essential to photonic sample-to-answer systems, significantly enhancing advancing preventive, personalized, and precision medicine.

The emergence of infectious diseases like COVID-19 (SARS-CoV-2), monkeypox, and avian influenza has threatened public health and global economies, with particularly severe impacts on low-income countries[1–3]. Significant advancements in infectious disease research and therapeutic development have been made to overcome these challenges, focusing on biosecurity, predictive and preventive medicine, and personalized healthcare. Among numerous technologies devoted to rapidly monitoring infectious diseases, plasmonic biosensors are a powerful tool because of their great specificity and sensitivity in sample collection and recognition. Plasmonic nanostructures or nanoplasmonic optical antennas (NOAS), typically made of metals, have the unique property to concentrate and couple with light for its oscillation and resonance of electrons on their surface[4,5] at highly localized hotspots. These hot spots in nanostructures generate a photothermal effect, benefiting the localized photothermal lysis of pathogens, exosomes, or cells, and enhancing nucleic acid amplification tests (NAATs) through photonic/plasmonic polymerase chain reaction (PCR) or isothermal methods[6] such as loop-mediated isothermal amplification (LAMP), rolling circle amplification (RCA), and recombinase polymerase amplification (RPA)[7–9]. NOAS also enable quantitative detection of molecules through their fingerprints by enhancing their vibrational and electronic excitations near its surface. Molecular fingerprints can be identified without labels using surface-enhanced Raman scattering (SERS)[10], plasmon resonance energy transfer (PRET), quantum biological electron tunneling (QBET)[11,12], reverse PRET[13], or the naked eyes (colorimetric detection)[14].

NOAS can be optimized to explore cellular environments[15] and monitor molecular dynamics[5]. Size, shape, and composition of nanoparticles can be designed with specific localized surface plasmon resonance (LSPR) wavelengths from the ultraviolet–visible (UV–vis) to the infrared (IR) region[16]. Various shapes offer different optical properties, including nanospheres[17], nanorods[18], nanoshells[19], nanocages[20], nanocrescents[21], and nanostars[22] (Box 1). Structures with sharp edges, like nanocrescents[23,24] and magnetic nanocrescents[25] with high electromagnetic field enhancement factors and near-IR (NIR) absorption, serve as alternatives for SERS substrates, and deeper penetration and reducing photothermal damage in biomedical imaging. Anisotropic nanostructures like nanorods, nanoshells, and nanocages with near-infrared LSPR are especially useful for photothermal therapy due to reduced light attenuation in biological tissues[26–31].

Plasmonic detection platforms offer stable solutions for identifying biological components at low concentrations or at the single-molecule level, which makes them ideal for early diagnosis and patient monitoring[32]. A thorough understanding of the physical chemistry of nanomaterials is crucial for designing molecular diagnostic systems that achieve ultra-fast detection, especially in infectious disease diagnostics, where quicker results can lower both time and costs in clinical environments.

This review highlights recent developments in plasmonic biosensors and actuators, designed to create advanced integrated molecular diagnostic systems that enable sample preparation and detection on a single chip. We investigate the principles of plasmonic trapping, the enrichment of biomarkers, and the design plasmonic nanostructures to improve photothermal lysis efficiency in biological samples. Furthermore, we address how these nanostructures contribute to ultrafast photothermal cycles in PCR for nucleic acid amplification. Finally, we examine label-free plasmonic biosensors and their potential applications for future ultrasensitive molecular diagnostics aimed at early diagnosis in preventive and precision medicine.

[1]Institute of Quantum Biophysics, Department of Biophysics, Sungkyunkwan University, Suwon, 16419, Republic of Korea. [2]Department of Intelligent Precision Healthcare Convergence, Sungkyunkwan University, Suwon, 16419, Republic of Korea. [3]Harvard Medical School, Harvard University, Boston, MA, 02115, USA. [4]Renal Division and Division of Engineering in Medicine, Department of Medicine, Brigham and Women's Hospital, Boston, MA, 02115, USA. [5]Department of Bioengineering, University of California at Berkeley, Berkeley, CA, 94720, USA. [6]Department of Electrical Engineering and Computer Science, University of California at Berkeley, Berkeley, CA, 94720, USA. ✉e-mail: kwchung@skku.edu; lplee@bwh.harvard.edu

Box 1 | Tuning the plasmon resonance of nanoparticles

At specific wavelengths, the collective oscillation of electrons in nanoparticles leads to significant total light extinction (absorption and scattering) in the spectrum. This behavior is influenced by the nanoparticle's material, size, shape, and dielectric environment[288].

Material composition significantly influences the intensity and spectral location of the LSPR. Noble metals like gold and silver[289] are commonly used due to their high free-electron densities and free electron-like conduction bands, which facilitate strong interactions with electromagnetic waves in the visible spectrum[290]. In contrast, other metals like aluminum and copper have limited utility due to oxidation, lower plasmonic efficiency, and restricted LSPR tunability[291,292]. Therefore, alloying metals or modifying the surface can help adjust LSPR properties[293].

Nanoparticle size also affects LSPR characteristics. Due to electromagnetic retardation, larger nanospheres cause redshifted resonance wavelengths, increased total extinction, and a higher scattering-to-absorption ratio[294–296]. For instance, the LSPR of silver nanospheres shifts from 400 nm to 500 nm as their size increases from 10 nm to 50 nm[295]. Conversely, smaller nanoparticles display sharper absorption peaks due to strong radiative decay[297]. However, nanoparticles smaller than 2 nm lack LSPR due to quantum confinement effects[298,299].

Shape also influences optical properties. Isotropic particles like nanospheres resonate at distinct visible wavelengths, while anisotropic shapes such as nanorods, nanostars, and nanoshells support multiple LSPR modes, extending into the NIR range. Gold nanorods have dual LSPR peaks, associated with longitudinal (redshifted) and transverse (blueshifted) modes, determined by their aspect ratio (AR) (length/width)[300–302]. Nanoshells and nanocages can be adjusted by shell thickness[91,303], cavity size, or porosity[304]. By increasing the gold (III) chloride solution ($HAuCl_4$) or iodine ion (I^-) concentration during synthesis, the LSPR can be redshifted to the NIR and the IR region in nanocages and nanostars[28,305], respectively.

Lastly, the surrounding environment and interparticle distances (in aggregates) can shift the LSPR wavelength, further affecting the optical properties of nanoparticles.

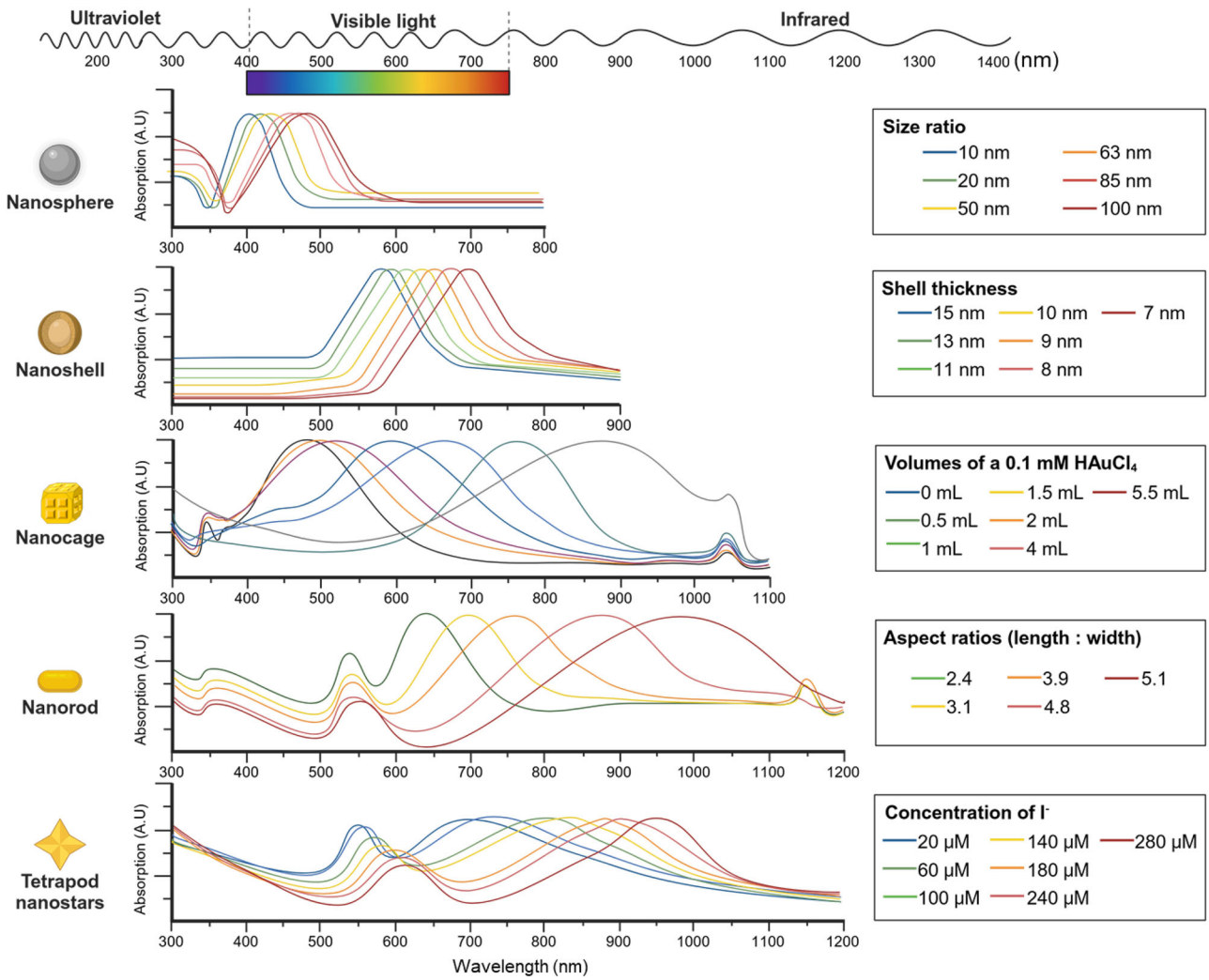

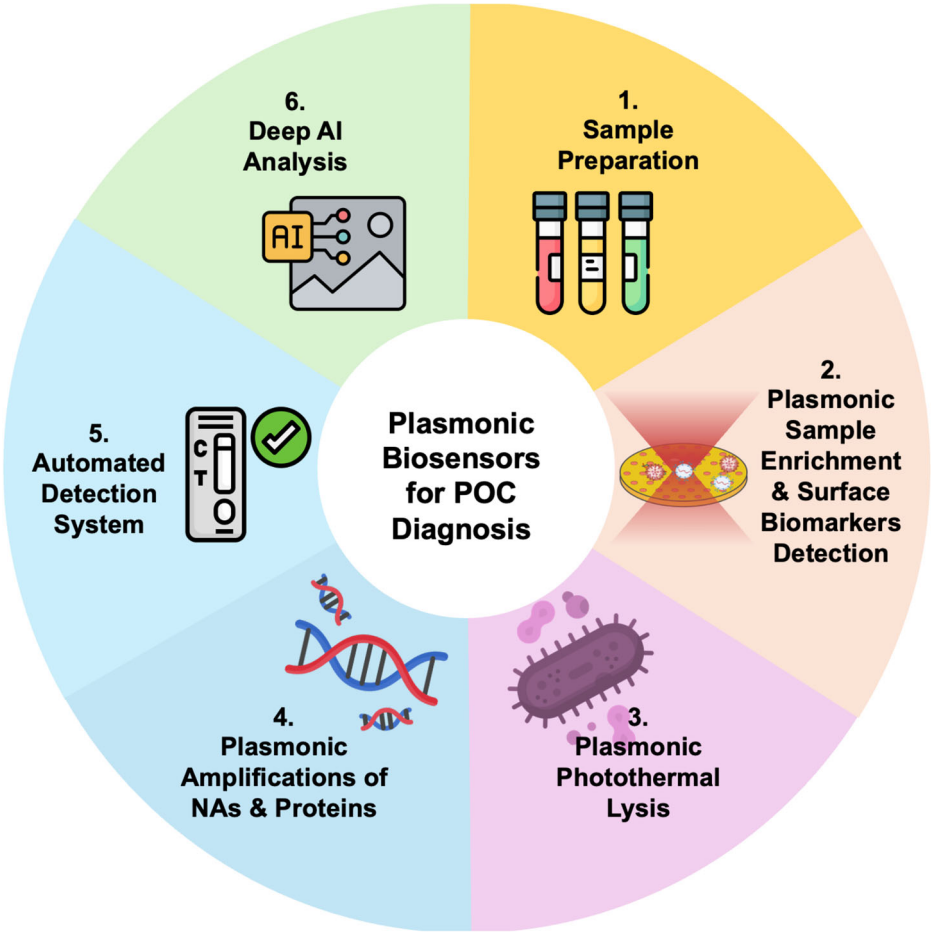

Fig. 1 | Complete biosensing process: from sample collection to data analysis for the diagnostic platform. In molecular diagnosis, biological samples such as blood, saliva, nasal swabs, or urine serve as biomarker sources for disease-related endogenous genes and infectious microorganisms. Nanoplasmonic optical antennas play a role in many biosensing applications, including sample collection, enrichment and purification, lysis, target amplification, and signal detection.

Biosensing workflow from sample-to-answer diagnosis

Biological samples such as blood, saliva, nasal swabs, or urine provide biomarkers for disease-related endogenous genes and infectious microorganisms at the molecular diagnostic level. In general, a comprehensive biosensing workflow for sample-to-answer diagnosis involves transforming biological samples into either qualitative or quantitative diagnostic results. This process incorporates several steps: (1) sample collection, (2) enrichment and purification, (3) lysis, (4) target amplification, (5) signal detection, and (6) data transmission. However, current chemical or mechanical sample preparation techniques are often time-consuming, non-selective, and damaging to delicate samples, which limit the purification yield of target molecules. Moreover, traditional biosensing methods, including NAATs, generally require large instruments and multiple sample preparation steps, and they exhibit a lower signal-to-noise ratio when dealing with complex clinical biological samples.

Conversely, plasmonic biosensing and actuation techniques are particularly suitable for miniaturized integrated platforms tailored for point-of-care (POC) diagnostics (Fig. 1). These methods can selectively enrich target molecules, execute one-step localized plasmonic photothermal lysis, enable efficient and ultrafast photothermal heat cycling for the amplification of nucleic acids, or incorporate optical detection combined with artificial intelligence (AI) analysis. They offer improved signal amplification and processing speed, positioning them as an alternative to traditional methods in various applications.

Plasmonic actuators for trapping and enriching nucleic acids, proteins, exosomes, cells, and pathogens

A refined method known as plasmonic optical tweezers allows capturing biomolecules such as nucleic acids, exosomes, cells and pathogens in low concentrations, greatly minimizing the requirement for extensive sample preparation equipment and chemicals. The optical forces involved in these trapping platforms arise from interactions between light and matter, mainly influenced by the scattering and gradient forces of the electromagnetic field[33–39] (Box 2).

The plasmonic effect of nanostructures[40] can improve optical trapping, significantly reducing the necessary optical power. Therefore, combining nanoplasmonic structures and optical tweezers can improve the force scale and potential well depth[41] for efficient optical enrichment of biological samples (Box 2c). Plasmonic nanostructures can be engineered to efficiently propagate light and concentrate it into a hotspot[36] (Box 2d). When a dielectric particle is located at position (r) near the plasmonic nanostructure surface, the intensified optical near-field promotes trapping near the gold pads. Simultaneously, the lateral scattering forces induced by the coupling of evanescent waves drag the particle along the surface[42]:

$$\langle F_{scat}(t)\rangle = -\frac{1}{2}\int_v dv\, Re\{i\omega_0 P(r,\omega_0) \wedge \mathcal{H}^*(r,\omega_0)\}$$

The particle size affects the resulting electromagnetic field distribution, creating an optical potential landscape $U_{\text{grad}}(R)$ which can impact the particle motion. This potential energy $U_{\text{grad}}(R)$ originates the gradient (or polarization) force, $\langle F_{\text{grad}}(t)\rangle$:

$$F_{\text{grad}}(t) = -\frac{1}{4}\int_v dv\,\{(\nabla \cdot P(r,\omega_0))E^*(r,\omega_0) + (\nabla \cdot P^*(r,\omega_0)E(r,\omega_0)\}$$

in which $P(r,\omega_0) = \frac{\epsilon(\omega_0)-1}{4\pi}\varepsilon(r,\omega_0)$ is the vector electric polarization, which correlates to the dielectric constant $\epsilon(\omega_0)$ of the material, the local

electric field $E(r, t)$ and magnetic field $H(r, t)$ created by the incident light. Then, a standard gradient relation expressed as:

$$F_{\text{grad}}(t) = -\nabla_R U_{\text{grad}}(R)$$

where the potential $U_{\text{grad}}(R)$ defined from the optical index n_{bead} of the particle material and the electric near-field intensity $|E(r,\omega_0)|^2$, is given by:

$$U_{\text{grad}}(R) = -\frac{n_{\text{bead}}^2 - 1}{16\pi}\int_v dv|\mathcal{E}(r,\omega_0)|^2$$

This potential depth can be actively tuned by altering the illumination wavelength $\lambda_0 = 2\pi c/\omega_0$ or the incident angle θ. A near-field plasmon resonance and thus the trapping potential can be significant amplified by the increasing the integral $\int_v dv|E(r,\omega_0)|^2$.

Two main strategies that can amplify optical forces on nanoparticles are using surface plasmons generated by manipulating metal nanoparticles to increase their mechanical response to the surrounding optical fields[43,44] or to create intensified fields[45]. The magnitude of light transmission is highly influenced by excitation light's wavelength and polarization, as well as the nanostructure's geometry and surrounding dielectric environment[46]. Typically, metallic structures are patterned on dielectric substrates containing target molecules in biological fluid samples. Among various geometries, plasmonic dimers, consisting of two identical metal nanoparticles separated by a nanogap, exhibit properties that concentrate propagating light beyond its diffraction limit[47–50]. When the propagating light and the particles are linearly polarized, it results in tight confinement and an intense light spot within the gap area[51] (Fig. 2a). During light exposure, plasmonic nanostructures undergo Joule heating due to the strong absorption in metals. The heating creates a temperature gradient at the interface between the nanostructure and its surrounding area, which depends on the power and time of irradiation. In fact, in nano-optical trapping, the temperature in a nanohole can increase by 10 °C by the illumination of moderate light intensity (2 mW/μm^2)[52] or illumination on a gold film at an intensity of 6.67 mW/μm^2 (at $\lambda_0 = 1064$ nm)[53]. The thermal effect can consequently disturb the stable trapping by speeding up diffusion and changing biological conformation[54] due to thermophoresis, convection, and thermos-osmosis[55]. The single nanohole structure exhibits a self-induced back action (SIBA) effect, in which the trapped object reinforces the restoring force within the trap[56]. The double nanoholes also dramatically enhanced field gradients at the inner-aperture junction to further create a sharper trapping potential[46,57,58] (Fig. 2b). Moreover, Crozier's group demonstrated a nano-optical tweezer based on all-silicon nanoantennas without deleterious thermal effect[59]. To achieve high-speed trapping and low concentration without perturbation of thermophoresis forces,

Box 2 | Optical tweezer mechanism

Optical tweezer or optical trapping is a force transducer that uses a diffraction-limited, tightly focused laser beam to trap and manipulate objects[306].

In the Rayleigh regime (particle size a ≪ λ), it responds to an electric field which is based on polarizability α. The particle's dipolar polarizability determines the magnitude of an optical field[307]:

$$\alpha = \frac{\alpha_0}{1 - \frac{ik^3\alpha_0}{6\pi\varepsilon_0}}$$

where $\alpha_0 = 4\pi\varepsilon_0 a^3(\varepsilon - 1)/(\varepsilon + 2)$[307]; k is the field wavevector; and ε_0 is the vacuum dielectric permittivity.

Hence, the optical forces can be calculated as[37]:

$$F = \underbrace{\frac{1}{4}\text{Re}(\alpha)\nabla|E|^2}_{\text{Intensity gradient}} + \underbrace{\frac{\sigma}{2c}\text{Re}(E\times H^*)}_{\text{Radiation pressure}} + \underbrace{\frac{\sigma c\varepsilon_0}{4\omega i}\nabla\times E\times E^*}_{\text{Polarization gradient}}$$

Where $\sigma = k_o Im\{\alpha\}/\epsilon_o$ denotes the particle's extinction cross-section, *E and H* represent the electric and magnetic field, respectively, c the speed of light in vacuum, and ω the angular frequency of the optical field. The first term represents the gradient force (F_{grad}) that pulls particles toward the high-intensity gradient of the electric field. The gradient force is proportional to the gradient of electromagnetic field intensity (I) $I = (\frac{1}{2})cn_m\varepsilon_o|E_0^2|$ and tends to reduce the energy associated with induced dipole:

$$\vec{F}_{\text{grad}} = \frac{\alpha}{4}\nabla|E_0^2| = (\frac{\alpha}{2}cn_m\varepsilon_0)\nabla I$$

The second term corresponds to the scattering force (F_{scat}) that pushes particles along the direction of light propagation caused by momentum transfer from light's absorption and scattering[306]:

$$\vec{F}_{\text{scat}} = \frac{n_m\sigma_{\text{ext}}}{2c}\text{Re}(E\times H^*) = \frac{n_m(\sigma_{\text{abs}} + \sigma_{\text{scat}})}{2c}\text{Re}(E\times H^*)$$

The third term represents a spin-induced force resulting from the presence of spatial polarization gradients (spin force is zero ($E \times E^* = 0$) for the linear polarized light).

To optimize optical traps for different particle sizes and laser powers, the gradient force and scattering force can be rewritten in terms of particle size (r) and laser intensity (I)[308]:

$$F_{\text{scat}} = \frac{128I_0\pi^5 r^6}{3\lambda^4 c}\left(\frac{N^2-1}{N^2+2}\right)^2 n$$

and

$$F_{\text{grad}} = -\frac{n^3 r^3}{2}\left(\frac{N^2-1}{N^2+2}\right)\nabla(|E|^2)$$

Where λ is the wavelength of the incident light, N is the object's refractive index relative to the medium, where n is the object's refractive index. In the Rayleigh regime, gradient and scattering forces scale with r^3, and r^6 respectively, so the gradient force usually dominates, pulling the particle toward the highest field intensity (Box 2a) or lowest potential (since $U \propto -|E|^2$); the trapping potential (U) depends on both the gradient force and particle size[308]:

$$U(r_0) = -\infty F_0\int F(r)dr$$

Where r represents a position in space, dr denotes an infinitesimal displacement. For a stable trapping, the potential well depth must exceed the particle's thermal energy (kT), typically requiring ~10kBT[55,309]. Since $U \propto r^3$, trapping smaller particles is more difficult and demands a higher light intensity gradient or tighter focusing beam[310] (Box 2b).

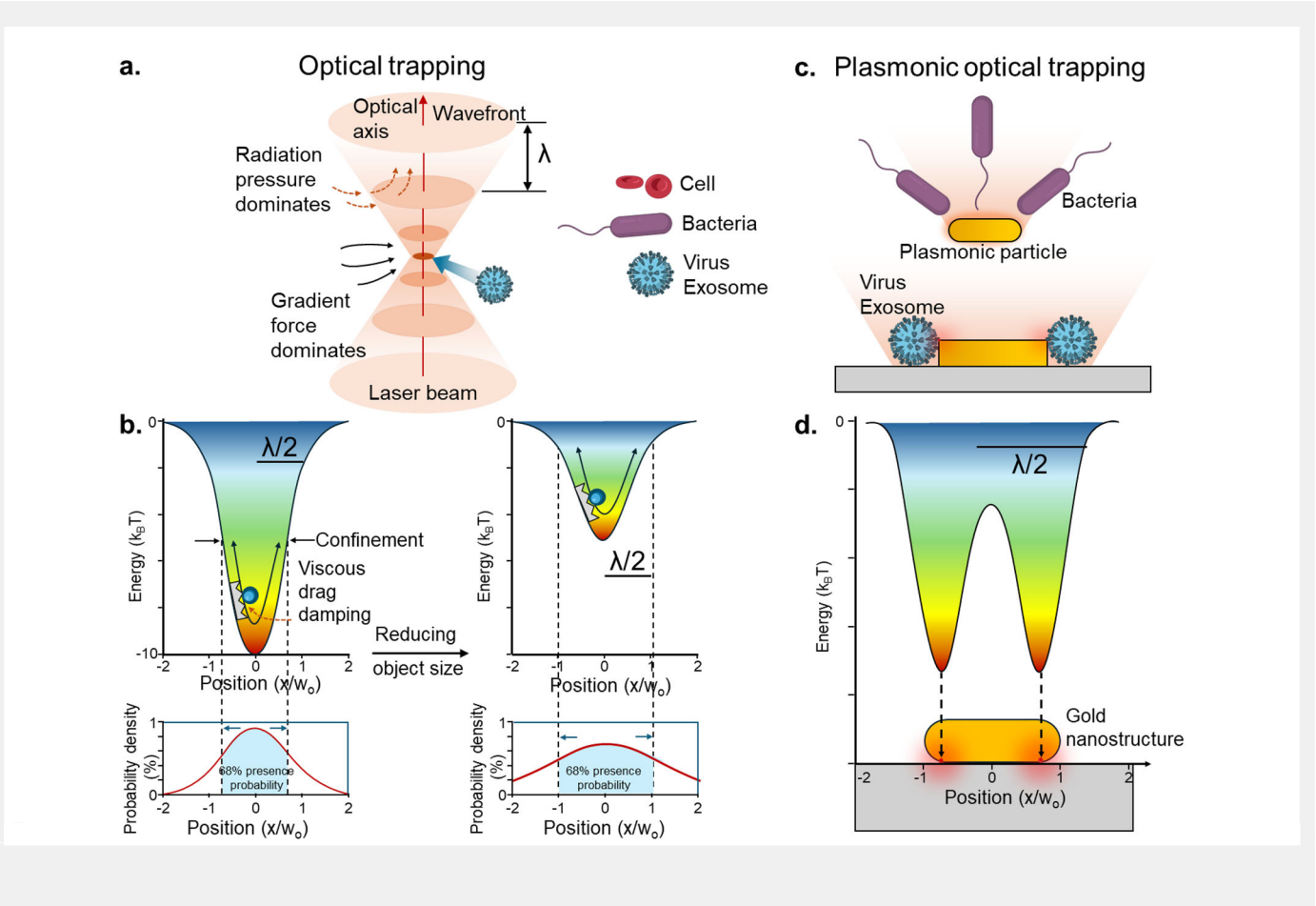

electrothermoplasmonic (ETP) effects, a combination of plasmonic heating with an a.c./d.c. (alternating current/direct current) electric field, induces the capturing and forcing of suspended particles to the trapping area on the timescale of a second. The a.c. field is then switched to a d.c. field or a low-frequency a.c. field <10 Hz to permanently lock the particles in the hotspot even when light illumination and d.c. field turning off[60]. By alter laminar flows in microfluidics, the ETP can be implemented in LSPR assay to accelerate the trapping of IgG to the sensor surface, resulting in improved sensitivity and faster detection time[61] (Fig. 2d). However, when the plasmonic heating is dissipated by high thermal conductivity substrate, the photothermal hotspot is eliminated, preventing ETP flow induced particle transportation[62].

Moreover, optical traps are typically constrained to small sample volumes. For low concentrations of biomolecules, exosomes, or pathogens, it may not ensure reliable trapping and detection. Whang et al. integrated a nanoporous mirror with hydrodynamic trapping to enhance bacterial enrichment on the nanopores of a plasmonic optical array (Fig. 2c). Strong near-field enhancement occurs due to focused light from interference and diffraction at the nanopore, nanoplasmonic particles attached and assembly on the bacterial surface, and interactions of a plasmonic mirror surrounding the nanopore. The diffraction of the incident light within the nanopore on gold film causes constructive interference that can amplify the electric field between gold nanoparticles and a gold film[35,47,63]. When a particle tries to escape, a reduction in light momentum (ΔT) generates a force (F) that draws the particle back into the nanopore[64]. Opto-hydrodynamic trapping, the combination of opto-hydrodynamic effect and optical trapping, is used for trapping different nanosized bio-samples such as viruses, mycoplasmas, and pathogenic bacteria[65]. Moreover, photothermal actuation of Marangoni flow allows microswarm robots to perform collective migration, self-organization and group rejection[66]. This microswarm technology has been applied to optothermal, damage-free gene delivery in biomedical applications[67]. Additionally, Xin's group introduced an opto-thermal-hydrodynamic approach for precise manipulation and flexible patterning of large-scale particle assemblies (up to 2000 particles) with a variety of shapes and sizes (0.5–20 μm)[68], as well as direct 4D patterning with single-particle resolution[69].

Although convection flow comes with the disadvantages of photothermal heating, photothermal-induced convection flow can be utilized to enhance the assembly of various colloids with different gram-positive and gram-negative bacteria (*E. coli*, *B. subtilis*, *B. cereus*, and *M. luteus)* for strengthening the SERS signal without the need of specific linker or templates[70] (Fig. 2e). The motions of colloids depend on sizes and densities under same velocities. Drag force pulls the small sub-100 nm molecules follow the convection flow by their density. As the size of the molecule increased, gravity and the buoyancy forces became more significant. Yet, when the molecule density was approximately equal to that of water, drag force dominated and controlled the transport. However, this method is still suffering from particle aggregation so that it is not sufficient to use for single particle trapping and fingerprint detection of a single biomolecule. Geometry-induced electrohydrodynamic tweezers (GET) are introduced as an ideal for massive single nanosized particles within seconds without detrimental heating at the hotspot (Fig. 2f). The GET platform uses a scalable circular array of plasmonic nanoholes with a central void to generate electrohydrodynamic potentials that trap single nanosized particles at the void center, while also enhancing fluorescence emission through surface plasmon waves[62]. The plasmonic photothermal forces enable applications such as particle separation[71–74], cell/colloid manipulation[75], extracellular vesicle (EV) analysis[76], DNA size manipulation[77], blood sorting[78], and bacteria separation[79].

Plasmonic optical trapping or plasmonic nanotweezers can become an alternative method for enrichment of biomolecules since they have the

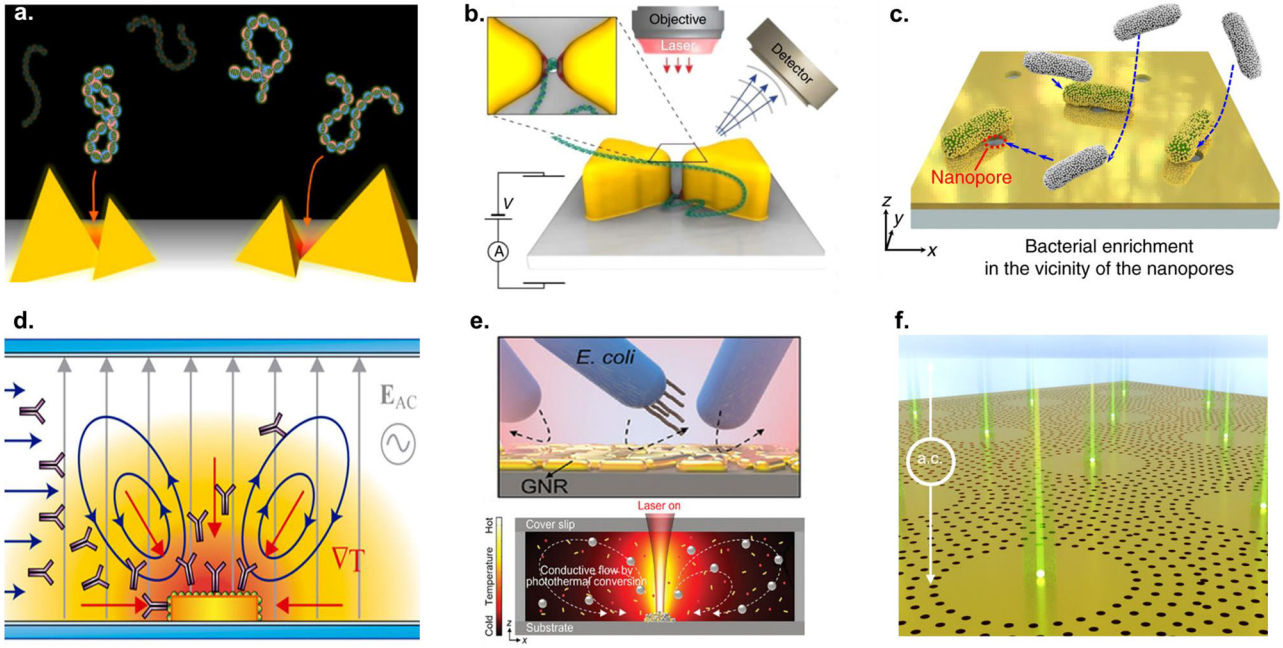

Fig. 2 | Plasmonic tweezers as actuators for selective trapping and enrichment of biological samples: DNAs, RNAs, proteins, exosomes, viruses, and pathogens. **a** Reversible trapping of lambda DNA on a metallic nanostructure by switching femtosecond-pulsed NIR laser irradiation on and off. Reprinted with permission from ref. 51. Copyright 2013 American Chemical Society. **b** The nanogap of a gold bowtie can create intense optical hot spots that trap DNA translocation through its nanopore, offering physical control over the speed of DNA movement. Reprinted with permission from ref. 54. Copyright 2015 American Chemical Society. **c** Plasmonic bacteria are forced to align on the nanopore. Reprinted with permission from ref. 285. Copyright 2018 Springer Nature. **d** An electrothermoplasmonic effect-based LSPR microfluidic sensing chip can overcome optoelectrical convection flow, demonstrated through high fluid velocities and improved immunoglobulin G detection performance. Reprinted with permission from ref. 61. Copyright 2018 American Chemical Society. **e** Thermophoretic force is created when photothermal heating around gold nanorods under resonant laser irradiation (785 nm) drives convection flow, enabling the localized plasmonic gold nanorods assembly with micro-sized bacteria without requiring specific linkers or templates. Reprinted with permission from ref. 70. Copyright 2022 Wiley-VCH GmbH. **f** Nanocavities of geometry-induced electrohydrodynamic tweezers (GET) allow a.c. electro-osmotic flow at the center of the void region where individual EVs are to be trapped, enabling plasmon-enhanced optical trapping under laser illumination without causing harmful heating effects. Reprinted with permission from ref. 62. Copyright 2023 Spinger Nature.

ability to overcome the diffraction limit for trapping and detection of biomolecules with low laser powers as well as chip device integration. Its application remains limited application from lab-to-industry due to complex fabrication methods, small trapping range and thermal effects although there are many efforts to overcome its limitations, including increasing inverse design, accurate trapping potential and perturbation, simplified instrumentation[80].

Enhanced lysis efficiency by nano-plasmonic structures

Photothermal heating does not necessarily have to be destructive when it facilitates a hotspot area. If the temperature surpasses the trapped particles, it can reshape the melt molecules into various forms depending on the power and illumination time. Biological membranes of exosomes, cells, or pathogens are highly vulnerable to heat, particularly within the range of 60–100 °C, which disrupts their structural integrity and functionality[81–84]. Therefore, the activation of nanoplasmonic photothermal lysis with localized heating up to 300 °C can effectively disrupt cellular membranes[85]. Moreover, metal nanoparticles are promising alternatives for antibacterial purposes due to their ability to produce reactive oxygen species (ROS) (·OH, $\cdot O_2^-$, and $^1O_2$), release cations, damage biomolecules, deplete ATP, and interact with bacterial membranes[86,87] (Box 3). As nanoparticle size decreases, their specific surface area increases, enhancing their interaction with the surrounding environment[88,89]. Bacterial cells interacting with polyvalent gold nanoparticles can lead to cell damage through two main pathways: (1) direct contact and (2) light-induced photothermal effect (Fig. 3a). A simple setup using LED illumination (excitation wavelength and exposure time) through focused beams that match the optical absorption of nanoparticles or nanostructures[90] can be coupled with LSPR[91–93] for localized photothermal heating. The stability of local heating can be achieved by controlling metallic nanostructures with less energy consumption[94]. Additionally, enhanced heating efficiency can be further achieved by controlling the geometry of nanoparticles (such as size, shape, and wavelength) and adjusting optical absorption at desired wavelengths[95–97] or by using a concise channel in a microfluidic chip to obtain efficient optical absorption. For instance, Fig. 3b shows gold nanoparticles embedded in the modified herringbone structure of polydimethylsiloxane (PDMS) microfluidic chips for bacteria trapping and DNA extraction. Bacteria captured were irradiated with a 532 nm laser for 10 minutes to complete the DNA extraction for the PCR process[98]. Using the same 532 nm laser in the lysis chamber containing magnetic particles, a 15 min irradiation can extract DNA from the foodborne pathogens[99]. Spherical gold nanoparticles were irradiated by white light laser beams to disrupt microbial membranes at 100 °C within 2 min[98]. Moreover, the excitation by blue LED (447.5 nm) on gold-coated polycarbonate membranes quickly disrupts the membrane proteins of *E. coli* at a temperature of 90 °C within 1 min, making them useful for point-of-care urinalysis (Fig. 3c). NIR lasers were used to irradiate high-aspect-ratio gold nanorods to achieve efficient localized photothermal bacterial lysing within 30 s[100]. Moreover, the highly efficient photothermal cell lysis chip (HEPCL chip) composed of PDMS chips and plasmonic gold nanoislands enables broad-spectrum absorption and can evenly distribute temperature across the chamber, reaching the optimal temperature for cell lysis within 30 s (Fig. 3e). The heating efficiency of gold nanoislands can trigger lipid membrane photoporation and successfully lyses 93% of PC9 cells at 90 °C while minimizing DNA denaturation[7]. Compared to continuous light, LED-pulsed plasmonic photothermal can extract enzymes and enhance the capability of detecting antimicrobial resistance enzymes like β-lactamase[101]. Using on-chip

Box 3 | Mechanism of photothermal lysis

Some metals, like zinc, silver, and copper, inhibit bacteria even in macroscopic form, while iron oxide can typically develop antibacterial activities only at the nanoscale[311]. When continuous waves or laser light are exposed to gold nanoparticles, they produce singlet oxygen ($^1O_2$), generating a photochemical reaction that can destroy the cells. The equilibrium of hot electrons correlated with $^1O_2$ photogeneration can be explained by Dexter-type electron exchange coupling[312,313]. One electron moves from an oxygen $2\pi^*$ orbital to a photogenerated hole on the sensitizer, while another electron of opposite spin transitions from a high-energy sensitizer level to the same or another $2\pi^*$ orbital, resulting in singlet oxygen in either the $^1\Sigma$ or $^1\Delta$[314,315]. For this process to occur, an oxygen molecule must be within ~10 Å of the nanoparticle surface at the instant of excitation to allow electronic wavefunction interaction[316]. These reactive oxygen species (ROS) cause oxidative stress, damaging bacterial membranes by targeting thiol groups in membrane proteins[317,318]. Moreover, nanoparticles release metal ions that disrupt the membrane by altering lipopolysaccharide structures, inducing lysis, and interfering with metabolic pathways[311].

Plasmon resonance relaxation in nanostructures can occur through two main pathways: radiative decay, where photons are re-emitted, or non-radiative decay, where hot electron–hole pairs are generated via Landau damping[110,319]. These hot carriers interact with metal lattice phonons, generating local heat. When photothermal heating raises membrane temperature above 41.4 °C[320], it converts the lipid bilayer from a gel[321] to a fluid phase[322]. This induces photoporation[323] and expansion among phospholipids, lowering membrane density and increasing permeability[324]. Water influx through the membrane causes swelling, disruption and eventual release of cellular components[325–327]. Interestingly, the membrane has intrinsic properties for self-repair under moderate heating. Brownian diffusion forces phospholipid molecules to move from higher concentrations to lower concentrations for the healing process[328].

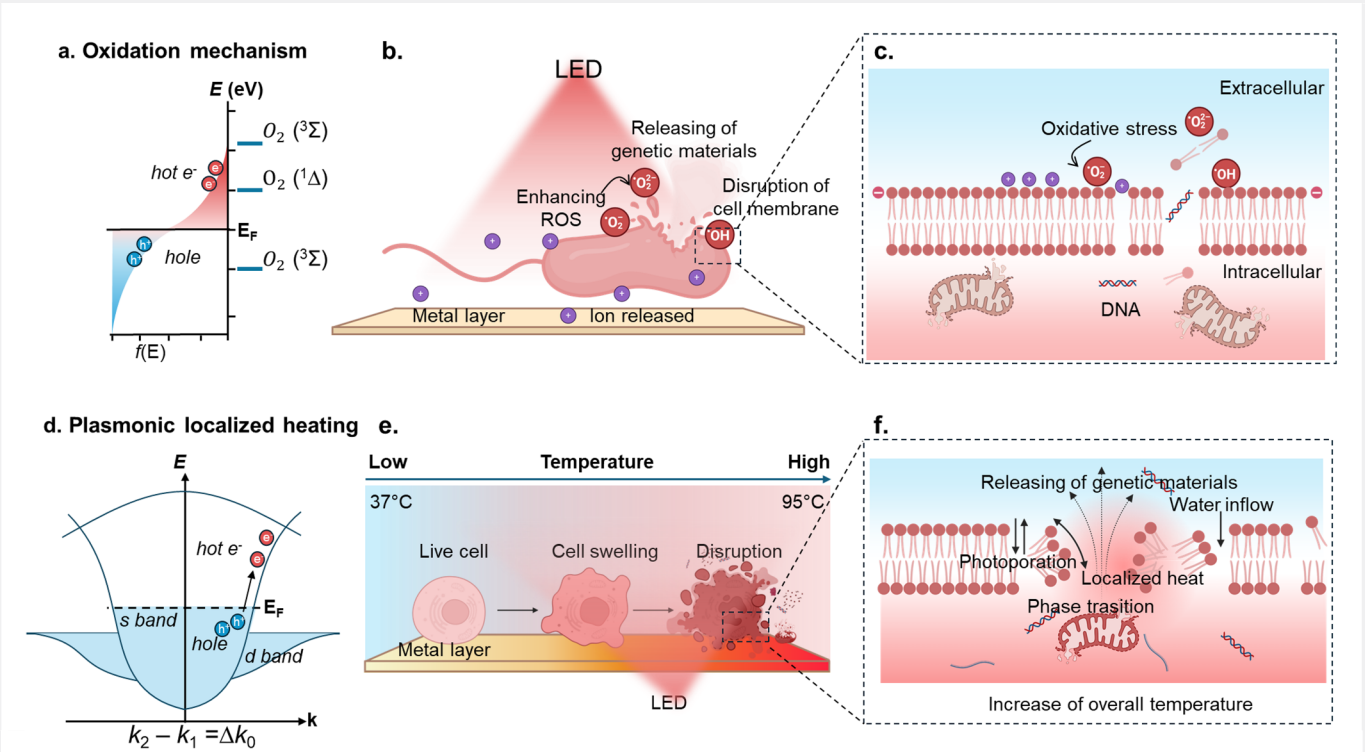

LED-pulsed plasmonic photothermal lysis achieves cell lysis without protein denaturation (Fig. 3f). However, photothermal heating can cause non-specific lysis of cells, mitochondria, bacteria, and vesicles, which may create unwanted background interference. This interference complicates downstream analysis and differentiates between target and non-target molecules in complex biological samples such as bodily fluids (e.g., blood, saliva, and urine) or tissue extracts. Moreover, photothermal heating can lead to uneven temperature distributions between the hotspot and surrounding areas, resulting in either partial lysis or complete breakdown of cellular components. To address this issue, it is essential to optimize optical power precisely to promote efficient lysis while minimizing excessive non-uniform heating. An appropriate sample pretreatment or purification step may also be necessary before photothermal lysis of cells and cellular components to ensure controlled and selective processing.

The multiple-element nanoparticles made of iron–nickel–copper (FeNiCu) selectively promote the release of ions to *E. coli* cell membrane protein groups, depending on metal binding affinity to membrane proteins. Specifically, copper ions were released significantly more than nickel, while iron showed the least release[102]. This highlights the potential of multi-principal element nanoparticles for controlled metal ion release in antibacterial applications (Fig. 3d). Recent focus has shifted toward leveraging the synergy between metals' surface plasmon resonance and semiconductors, broadening LSPR and enabling the excitation of adjacent semiconductors[103,104]. By semiconductor supports, hot electrons generated from plasmonic metals are transferred to semiconductors under incident light and extending the lifetime of these hot carriers[105]. For example, an interfacial bismuth sulfide/titanium carbide MXene ($Bi_2S_3/Ti_3C_2T_x$) Schottky junction showed intense photocatalytic activity under near-

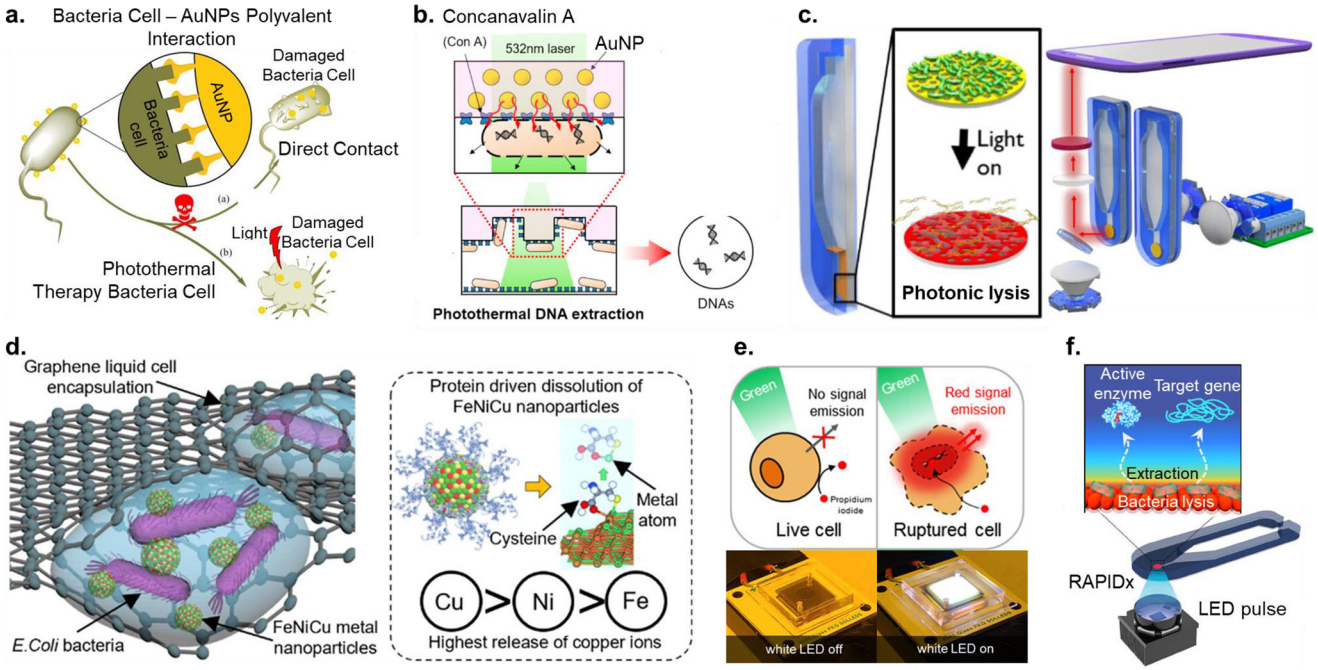

Fig. 3 | Plasmonic lysis effects of nano-plasmonic structures. a Schematic diagram illustrating the mechanism of cell disruption by the oxidative mechanism through two main pathways: (1) direct contact and (2) light-induced photothermal effect. Reprinted with permission from ref. 286. Copyright 2019 Wiley-VCH Verlag GmbH & Co. KGaA, Weinheim. **b** Gold nanoparticles embedded in conjunction with a modified herringbone-structured GASI microfluidic chip to capture, enrich, and extract their DNA via a 532 nm laser with a power of 300 mW for 10 irradiations. Reprinted with permission from ref. 98. Copyright 2017 Elsevier B.V. **c** Gold-coated nanoporous membrane enables 40,000-fold bacterial enrichment from a 1 mL sample in 2 min and photothermal lysis of bacteria within 1 min through ultrafast light-to-heat conversion. Reprinted with permission from ref. 8. Copyright 2019 American Chemical Society. **d** Multi-principal element nanoparticles (FeNiCu) show the release of metal ions (Cu, Ni, and Fe cations) with different binding affinity to bacterial cell membrane protein functional groups, leading to the disruption of bacterial walls. The release of ions decreased from copper to nickel and then to iron. Reprinted with permission from ref. 102. Copyright 2023 American Chemical Society. **e** Strongly absorbed plasmonic gold nanoislands (SAP-AuNIs) generate uniform photothermal heating, achieving rapid cell lysing 93% of PC9 cells at 90 °C in 90 s without nucleic acid degradation. Reprinted with permission from ref. 7. Copyright 2023 American Chemical Society. **f** A **r**apid **a**ntimicrobial-resistance **p**oint-of-care **i**dentification **d**evice (RAPIDx) can extract contamination-free active target enzyme by photothermal lysis of bacterial cells on a nanoplasmonic functional layer on-chip without destroying the enzymatic activity by pulsed LED. Reprinted with permission from ref. 101. Copyright 2024 Wiley-VCH GmbH.

infrared radiation by facilitating charge transfer, thereby increasing electron density, and consequently generating reactive oxygen species, then enhancing bacteria membrane permeability[106]. The antibacterial efficiency was up to 99.86% against *S. aureus* and 99.92% against *E. coli* within 10 min; moreover, plasmon excitation of gold nanorods distributed on titanium dioxide (TiO_2) nanosheets can induce light-driven production of hot electrons and ROS for broad-spectrum photocatalytic activity[107]. However, the substantial ROS can disrupt biomolecules and organelle structures, leading to DNA/RNA damage[108,109]. Therefore, precise control of nanoparticle design and light irradiation is necessary to maintain the cellular components for further diagnosis. Oxidative reactions from plasmonic lysis can produce unwanted byproducts like lipid peroxidation and protein oxidation. These reactions may also cause structural changes, jeopardizing biomolecular integrity, leading to false-negative results in follow-up analyses. In addition, biological systems contain inherent antioxidants and reducing agents that can neutralize ROS or aid in molecular repair, which can markedly reduce overall lysis efficiency. Like photothermal heating, ROS-mediated plasmonic lysis can cause non-specific cell damage and inconsistent efficiency, necessitating thorough optimization and purification to achieve selective and reproducible results.

Nano-plasmonic structures enhanced nucleic acid amplification

Photothermal heating involves four primary steps, occurring within a timescale of ~100 ps[110–113]. First, when a photon from an incident light reaches and is absorbed by the metal nanostructures, a generation of electron-hole pair is generated, exciting electrons and holes and driving them out of equilibrium. Next, these exciting, high-energy carriers undergo thermalization by the relaxation of energy through electron-electron scattering. Then, these electrons dissipate their thermal energy into the lattice by electron–phonon interaction. Finally, this lattice energy dissipates into the surrounding environment[114–117] (external thermalization) (Fig. 4a). Electron thermalization occurs extremely quickly in bulk metals (500 fs for gold and 350 fs for silver)[115,118], making plasmonic photon-to-heat conversion adequate for use in NAAT application. In a subsequent study, mixing gold nanoparticles into bulk solution[119,120] improved PCR sensitivity[121] and reduced reaction time to 10 min[122] (Fig. 4b). In 2017, a remarkable achievement of 30 thermal cycles in just 54 s was accomplished by incorporating plasmonic gold nanorods (aspect ratio 4.1) using an 808 nm NIR laser (2 W) to photogenerated heating[123]. During the COVID-19 pandemic, Cheong et al., by integrating magneto-plasmonic nanoparticles having a diameter of 16 nm illuminated by an 80-mW laser diode wavelength of 532 nm with a portable device, could detect SARS-CoV-2 RNA in 17 min[124]. Integrating ultrafast photonic PCR with microfluidic platforms for point-of-care devices has involved extensive research on thin metal films[125] to accelerate amplification by minimizing sample volume and improving heat transfer rates. Son et al. used a thin gold film (65% absorption, 120 nm thick) as a photothermal heater for achieving 30 cycles within 5 min (Fig. 4c). Then, two gold films form optical mirrors to increase the photothermal heating efficiency and increase the sensitivity up to 2 DNA copies (cp)/μL[126]. Plasmonic pillar arrays, which absorb the light at the whole visible range, can induce the photogenerated heating for photonic PCR[127,128] (Fig. 4d). Photonic PCR is an effective solution for nucleic acid amplification, reducing amplification time, improving accuracy, and lowering costs through integrated plasmonics-based optofluidics and a low-cost complementary metal-oxide-semiconductor (CMOS) sensor. Controlling photothermal heating requires careful material selection, choice of light source, and integration

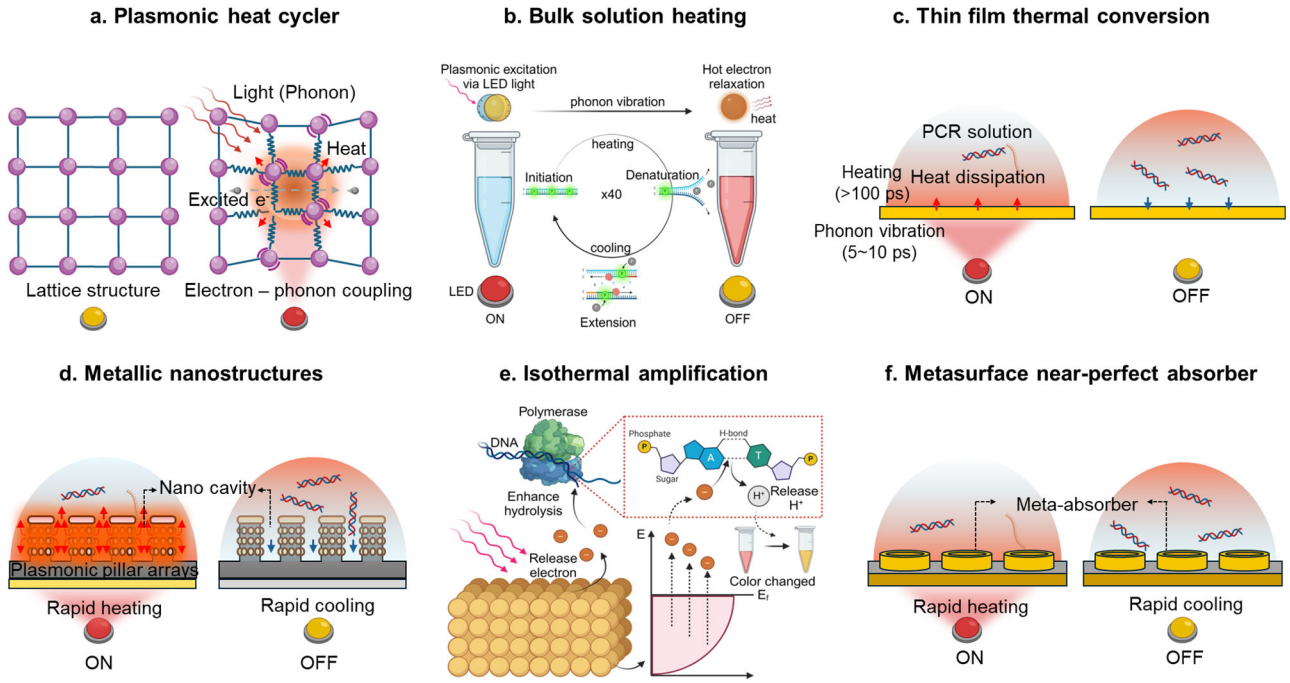

Fig. 4 | Plasmonic nucleic acid amplification. **a** Electron–phonon coupling leads to lattice heating. This coupling causes energy transfer. **b** Schematic illustration of nucleic acid amplification in bulk solution when switching the LED on and off. **c** Schematic illustration of nucleic acid amplification in a nanofilm. **d** Schematic illustration of nucleic acid amplification in nanopillar structure. **e** Schematic illustration of plasmon-enhanced colorimetric detection in isothermal amplification. **f** Schematic illustration of nucleic acid amplification in a metasurface near-perfect absorber.

with microfluidic chips (Table 1). However, current university-level demonstrations are underdeveloped and often perceived as expensive systems, primarily due to limited experience with integrated circuits and photonics within existing educational frameworks. As a result, students and postdoctoral researchers lack opportunity to gain experience comparable to that of professional device engineers in the industry. Skilled engineers can mass-produce integrated optofluidics and CMOS sensors, creating low-cost POC devices suitable for both developed and low-resource settings.

A plasmonic colorimetric sensing strategy was developed as a simpler approach for rapid integration with a photonic PCR-based POC device. For example, Jiang et al. introduced a direct detection plasmonic PCR method by combining magnetic nanoparticles and gold nanoparticle-based cross-linking colorimetry, achieving the limit of detection (LOD) of 5 copies/μL within 40 min[129]. Additionally, AbdElFatah et al. developed a microfluidic cartridge for plasmonic LAMP and RCA with colorimetric detection (Fig. 4e)[14]. In this system, hot electrons are generated from the self-assembled plasmonic nanoparticles (400 nm), accelerating nucleophilic reactions during the amplification process. As a result, protons were significantly produced, leading to a rapid decrease in pH, causing a color transition from fuchsia to yellow. Moreover, to enhance the sensitivity of colorimetric signals, they combined them with machine-learning algorithms to analyze the readout. This algorithm is designed to interpret the color changes quantitatively, determining whether the results are positive or negative for the target nucleic acids[14]. This method can amplify nucleic acids within 10 min, making it suitable for POC testing. As an alternative to thermal cycling-based PCR, isothermal amplification methods with a wide range of temperatures can be performed using an inexpensive and simple heating device. However, they still achieve the detection of single RNA copies per reaction. Despite their technological advancements in nucleic acid detection, these methods are limited in protocol standardization and still suffer from inconsistency[130], false positive results[131], complicated multiple primer sets[132], low amplification efficiency, and non-specific amplification[133]. Therefore, aside from LAMP, other isothermal amplification methods have experienced delayed US Food and Drug Administration (FDA) approval as primary diagnostic tools, while PCR remains the gold standard for NAATs.

One of the major limitations in enhancing light-to-heat conversion efficiency in photonic PCR devices is the light absorption of nanostructures[134]. Therefore, optimizing photothermal heating mainly focuses on tuning their plasmonic properties for enhancing light absorption and increasing electron–phonon coupling. A near-perfect absorber for an ultrafast metaphotonic PCR chip was recently introduced by Kim et al. as illustrated in Fig. 4f. A large-area titanium nitride (TiN)-based broadband meta-absorber on a 6-in. wafer can enable ultrafast DNA amplification within 6 min and 30 s using a compact single IR LED source operating at 940 nm with a power of 3.8 W. TiN offers significant advantages for photothermal heating over conventional plasmonic materials by increasing electron-electron scattering rise time (~115 fs) compared to gold (~1 ps), enabling quicker electron excitation. Moreover, TiN exhibits a 25–100 times stronger electron-phonon coupling than gold, resulting in a shorter thermalization time (0.15 ps versus 5–10 ps for gold) and a greatly enhanced photothermal effect[135]. Enhanced light absorption in nanostructures has led to the development of commercial photonic PCR systems now available on the market.

Plasmonic structures enhance optical detection for molecular diagnosis

For accurate molecular profiling, optical plasmonic antennas identify target molecules through their unique vibration and electronic excitations. By coupling optical antennas with target biomolecules, real-time and quantitative detection can be achieved through the corresponding spectra (Box 4).

Surface plasmon resonance

Surface plasmon resonance (SPR) is an optical sensing technique based on the excitation of surface plasmon polaritons, electromagnetic waves

Table 1 | Plasmonic photothermal cycles for the amplification of NAs

Materials	Speed	Reaction volume	Light source	Absorption (nm)	Heating rate (°C/s)	Cooling rate (°C/s)	LOD	Target	Year
Spherical gold nanoparticles (60 nm)	10 min	25–40 µL	532 nm laser, 3 W	532 nm	7.62	3.33	–	Human androgen receptor gene	2012 (ref. 122)
Gold nanorods (AR 6)	1 h/48 cycles (96 °C, 60 °C, 78 °C)	–	808 nm, 3.6 mW	781 nm	–	–	–	–	2013 (ref. 278)
120 nm gold film	5 min/30 cycles (55 °C, 95 °C)	5 µL	450 nm, 3.5 W	450 nm	12.79	6.6 with cooling fan	0.1 ng/µL	λ-DNA	2015 (ref. 279)
10 nm and 120 nm gold films	4 min/30 cycles (94 °C, 68 °C)	1.3 µL	447.5 nm, ≈20 W	300–500 nm	7.5	6.35	2 DNA cp/µL	c-MET cDNA	2016 (ref. 126)
Gold nanorods (AR 4.1)	54 s/30 cycles	10–25 µL	808 nm, 2 W	808 nm	70	50	1–50 ng	DNA	2017 (ref. 123)
PEGylated and silica-coated gold bipyramid (PEG-Si-AuBPs)	7.5 min/cycle	10 µL	IR-LED, 8.5 W	846 nm	16.6	9.4	5 ng/µL–1 pg/µL	M13mp18 DNA	2017 (ref. 280)
Polycarbonate membranes - 5 nm Titanium - 80 nm gold film	10 min/40 cycles (95 °C and 60 °C)	–	447.5 nm, 890 mW	447 nm	–	–	10^3 CFU/mL	*E. coli*	2019 (ref. 127)
Glass nanopillar array (180 nm) with 10 nm Ag coating and 40 nm Au nanoislands (GNA@Ag/AuNIs)	–	15 µL	white LED, 3–7.5 W	<500 nm	9.3	12.4	0.1 ng/µL	cDNA	2020 (ref. 127)
6 nm magnetic core covered by a 12 nmgold shell	42 °C (5 min), (40 cycles/6 min), signal detection steps (3 min)	20 µL	532 nm, 80 mW	535 nm	13.17	4.94	3.2 cp/µL	SARS-CoV-2	2020 (ref. 124)
150 nm iron oxide–gold (Fe_3O_4@Au) core–shell magnetic nanoparticles	<5 min	10 µL	850 nm, 8.5 W	850 nm	7.69	5.89	90 aM naked eyes	λ-DNA	2021 (ref. 120)
Glass nanopillar array (180 nm) with 10 nm Ag coating and 40 nm Au nanoislands (GNA@Ag/AuNIs)	3 min/40 cycles	1 µL	White LED, ~2.8 W	400–500 nm	11.95	7.31	1.37×10^4 cp/µL	SARS-CoV-2	2021 (ref. 128)
30.0 nm gold core–45.9 nm silver nanoshells	LAMP, ≈ 75 min	50 µL	heat blocks	≈530 nm	–	–	10 cp/ reaction	SARS-CoV-2	2022 (ref. 281)
Gold nanorods (AR ~ 4.5 nm) with 10 nm silica coating	2 min/Reverse transcription (RT) (2 min), denaturation (95 °C/10s), <15 min/45 cycles (60 and 95 °C)	20 µL	3 IR- LEDs	~850 nm	6.7	~4.7 with 12 V fan	5.9×10^3 cp/µL	SARS-CoV-2 RNA	2022 (ref. 119)
N-heterocyclic carbene (NHC)-conjugated gold substrate	8 min/40 cycles (60 to 95 °C)	–	Blue light	450 nm	8.75	17.5	843 cp	SARS-CoV-2	2023 (ref. 282)
Polystyrene particles covered by zinc oxide and aluminum	LAMP, lysis (3 min),detection (10 min)	130 nL	Ambient light	–	–	–	~5.3 cp/µL DNA	SARS-CoV-2, influenza A	2023 (ref. 14)
Nanoscale gold islands	Thermal lysis (3 min); RT–RPA (30 min); and hybridization on pGOLD (1 h)	40 µL	643 nm, 25 W	NIR	–	–	10 cp/ reaction	SARS-CoV-2 S gene	2023 (ref. 201)
Glass nanopillar array (180 nm) with 10 nm Ag coating and 40 nm Au nanoislands (GNA@Ag/AuNIs)	10 min (RT (210 s) and 400 s/40 cycles)	2 µL	White LED, 168 mW/mm^2	High absorption in the visible spectrum	18.85	8.89	10 cp/µL	SARS-CoV-2 RNA	2023 (ref. 283)
Plasmonic cavity membrane composed of gold nanorods with SiO_2 tips	3 min/30 cycles (55–95 °C)	1 nL	785 nm, 3.8 W	NIR	23.3	–	1 cp/µL	SARS-CoV-2	2024 (ref. 284)
Metal–insulator–metal (TiN ring structure, SiO_2 layer, a TiN film)	6 min 30 s/30 cycles (65–95 °C)	4 µL	940 nm, 3.8 W	Broad absorption spectrum	16.66	7.77	–	λ-DNA	2024 (ref. 135)
80 nm gold film	RCA, 40 min	–	Pulsed 447.5 nm, 0.75 W	–	–	–	10^3 CFU/ mL	β-lactamase-producing *E. coli*	2024 (ref. 101)

that propagate along a metal-dielectric interface. SPR is used to measure the changes in the refractive index near the metal surface, typically at interfaces with media such as liquid or air[136] (Fig. 5a). In SPR-based molecular detection, the sensing surface was immobilized with specific bioreceptors such as antibodies, DNA probes or ligands, which selectively bind to the target molecules. When the target molecules bind to immobilized bioreceptors, this leads to a change in refractive index, then causing spectra or angular shift[137,138]. SPR is known as a label-free method, which allows binding kinetics measurement and offers high sensitivity down to pg/µL[139]. Commercial SPR-based sensors are being developed for real-time monitoring of viruses[140,141], proteins[142], DNA[143], exosomes[144]. SPR is considered a surface-sensitive technique; however, its primary limitations stem from surface interactions. One significant drawback is the non-specific signal response, which arises from the broad region of the evanescent field (~100 nm)[145], whereas typical protein analyte sizes range only from 2 to 10 nm[146]. This discrepancy can result in non-specific signals from unintended contributions of molecules in the surrounding medium rather than actual surface-bound

Box 4 | The hierarchical structure of the energy levels of molecules

A molecule's energy levels include electronic (E_e), vibrational (E_v) and rotational (E_r) components, as described by the Born–Oppenheimer approximation. These energy levels of the ground state and excited state are illustrated by Perrin–Jablonski diagram, which shows energy transitions between the ground state (S_o), first (S_1), and second (S_2) excited states of the singlet electronic manifold. At ambient temperature, most molecules reside in the lowest electronic singlet state (ground state). When irradiated with light of an appropriate wavelength, they can be excited to a higher energy state. These excited states include electronic, vibrational, and rotational states. Ultraviolet and visible wavelengths (photon energy 5×10^4 to $1 \times 10^4\,cm^{-1}$) excite a molecule into its electronically excited state. The infrared region (photon energy 4×10^3 to $1 \times 10^2\,cm^{-1}$) and the microwave region (photon energy 2 to 0.5 cm^{-1}) are used to excite a molecule to its vibrational and rotational excited state, respectively[329]. During a spectroscopic transition (absorption and emission), the total energy absorbed or emitted is equal to the photon energy, expressed as:

$$h\nu = \Delta E_e + \Delta E_v + \Delta E_r$$

where $h\nu$ is the photon energy and each ΔE represents the change in respective energy level[330].

Molecular spectroscopy utilizes these transitions to probe molecular properties. Rotational motion energy levels allow molecular geometry determination, as these levels are directly related to the molecule's moment of inertia, which depends on internuclear distances. Electronic transitions in the UV–vis region provide structural information about molecules in both ground and excited electronic states. In plasmonic systems, light irradiation can excite surface electrons near the Fermi level (E_F) into the sp-band. These hot electrons can overcome the potential barrier and tunnel into nearby molecules, promoting electronic transition into the excited state ($|e>$)[9,331] (LUMO: lowest unoccupied molecular orbital, HOMO: highest occupied molecular orbital).

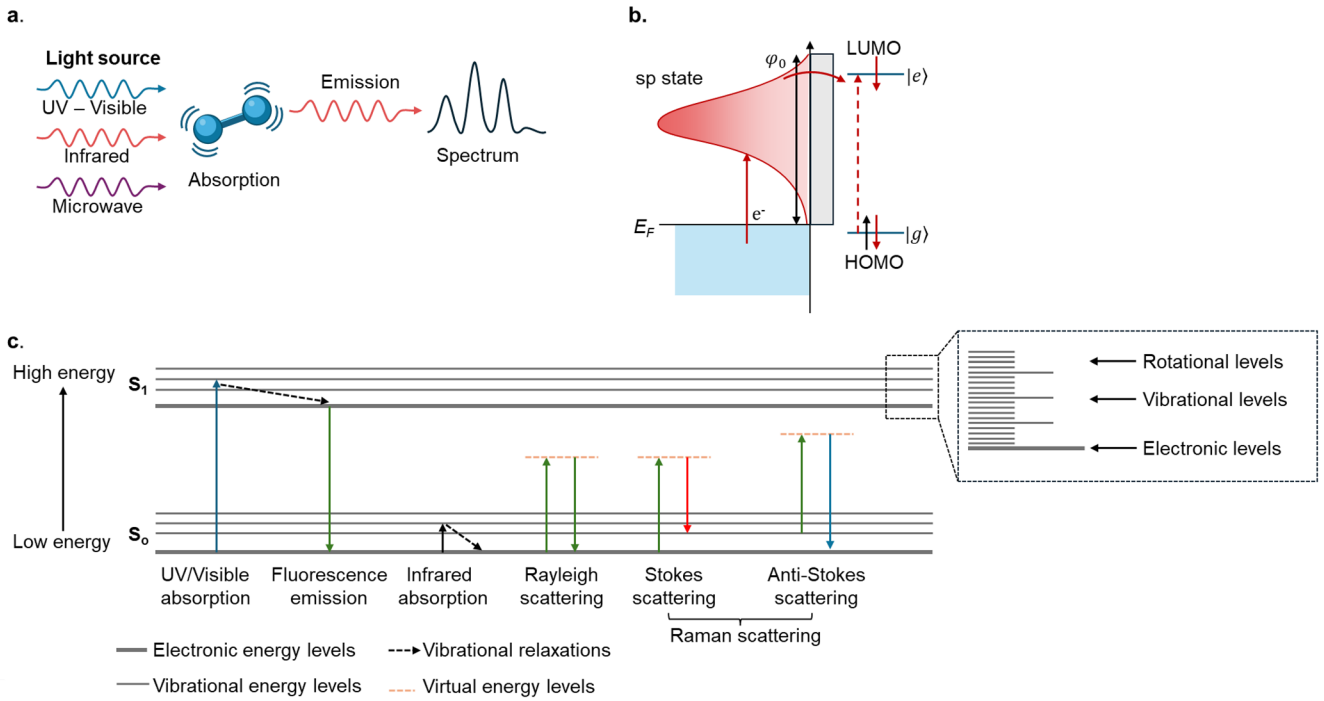

interactions. Additionally, shifts in the bulk refractive index in complex biological samples can induce a bulk response, leading to false-positive or misleading signals. Addressing this issue has driven considerable research efforts, including modulating the total internal reflection (TIR) angle to optimize surface interactions and utilizing polymer brushes under physiological conditions[147]. Developing robust strategies to eliminate bulk response remains essential for enhancing the specificity and accuracy of SPR-based biosensing.

Localized surface plasmon resonance

Localized surface plasmon resonance (LSPR) arises from the collective oscillation of free electrons throughout the entire metal nanostructure, leading to strong light absorption at specific wavelengths (Fig. 5b). In LSPR, the electromagnetic field decays exponentially with a length of approximately 5–10 nm, which is highly sensitive to the refractive index of the solution near the surface. Compared to SPR, LSPR offers higher spatial resolution due to the nanoscale confinement. This characteristic enables the development of refractive-index-based LSPR in biosensing fields[148]. This resonance, which depends on the refractive index, can be understood through the electrical resonance of an *LCR* circuit made up of an inductor (L), a capacitor (C), and a resistor (R). In this framework, the inductance is attributed to the material properties, the fringe capacitance is linked to the displacement current caused by the dipolar field interacting with the surrounding medium, and the resistance represents the limitations on electron oscillations at the surface[147]. In this model, the metal nanoparticle can be considered a nanoinductor, and the surrounding medium as a nanocapacitor, with capacitance directly related to the refractive index of that medium. The resonance frequency in electrical circuits is inversely proportional

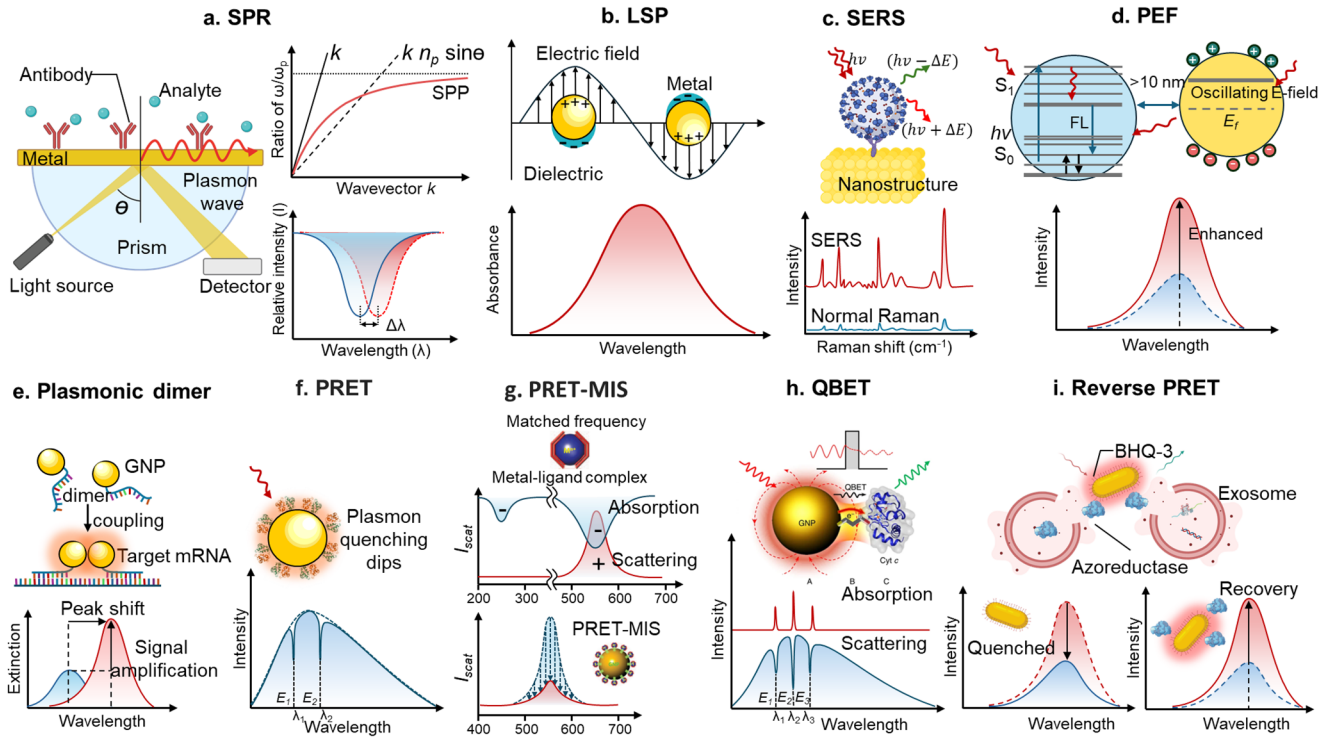

Fig. 5 | Plasmonic enhanced optical detection methods. a Schematic illustration of the surface plasmon resonance (SPR). SPR uses light-excited surface plasmon polaritons (SPPs) to detect the binding of ligands to receptors immobilized on a metallic thin film surface. **b** Schematic illustration of the localized surface plasmon resonance (LSPR). LSPR refers to the collective oscillation of conduction electrons near the surface of metallic nanostructures when exposed to light, generating a localized electromagnetic field with unique optical properties. **c** Schematic illustration of surface-enhanced Raman spectroscopy (SERS). The detected Raman shift is correlated to the excited vibration of the molecule, occurring during the inelastic scattering of photons (Stokes or anti-Stokes). **d** Schematic illustration of plasmon-enhanced fluorescence (PEF). The plasmonic nanoparticles enhance the local electromagnetic field, increasing the excitation rate and the radiative decay rate of the fluorophore nearby. **e** Schematic illustration of plasmonic dimer. Plasmonic coupling can enhance 10^4 stronger intensities than that of fluorophore molecules. **f** Schematic illustration of plasmon resonance energy transfer (PRET). Energy is transferred from plasmonic optical antennas to the molecule showing the quantized quenching dips at the absorption peaks of the molecule on the scattering spectrum of the nanoplasmonic optical antennas. **g** Schematic illustration of plasmonic resonance energy transfer-based metal ion sensing (PRET-MIS). Metal ions can be identified explicitly by conjugated metal–ligand complexes and a single gold nanoparticle using PRET-MIS. When the absorption spectrum of the metal–ligand complex matches with the scattering spectrum of the gold nanoparticle, it induces energy transfer, resulting in a distinguishable quenching dip on the gold nanoparticle scattering spectrum. Reproduced with permission from[230]. Copyright 2009 Springer Nature. **h** Schematic illustration of quantum biological electron tunneling (QBET). QBET spectroscopy uses PRET to observe real-time optical detection of quantum biological electron tunneling and electron transfer in mitochondrial cytochrome c during cellular apoptosis and necrosis in living cells. **i** Schematic illustration of reverse plasmon resonance energy transfer (rPRET). Monitoring dynamic intercellular communication can be achieved by interfacing plasmonic nanoantennas with resonating black hole quencher (BHQ-3) molecules, enabling cell–cell signaling detection through enzymes like azoreductase released via EVs or microvesicles (MVs).

to $(LC)^{1/2}$, which parallels plasmon resonance. Consequently, the plasmon resonance frequency rises as the refractive index of the surrounding medium drops. Diverse nanoplasmonic structures with different sizes and shapes are used to enhance the sensitivity of LSPR biosensors and maximize the $\Delta\lambda$ (wavelength shift) upon biomolecule interactions[149,150]. The enhancement from plasmonic nanostructures has improved LSPR-based detection of biomolecules such as ATP[151], proteins[152–154], exosomes[155].

Moreover, the LSPR-based technique can be integrated with lateral flow-based POC sensing devices that rapidly perform colorimetric detection[156–158]. Compared to conventional SPR, LSPR provides an advantage due to its high aspect ratio, enhancing the surface area for biomolecular interactions and improving compatibility with complementary detection methods, including SERS and surface-enhanced fluorescence (SEF)[140,159]. While LSPR offers certain benefits, it typically exhibits lower sensitivity to refractive index changes than conventional SPR. Nonetheless, its higher aspect ratio allows for enhanced accommodation of biomolecules on the surface of metal nanoparticles, which in turn boosts detection sensitivity. Recent studies have explored SPR–LSPR hybrid systems to optimize sensor performance[140]. Although LSPR shows significant potential for POC biosensing, it encounters hurdles like low selectivity in complex biological fluids, challenges in detecting membrane-associated species, and issues with integration in multiplexed platforms and POC devices. Tackling these obstacles is vital for the progress of LSPR-based biosensing technologies.

Surface-enhanced Raman scattering

Surface-enhanced Raman scattering[160,161] is an enhancement technique where Raman scattering (vibrational excitation) signals of molecules adsorbed on nanoplasmonic surfaces are amplified by up to several orders of magnitude (Fig. 5c). The scattering shift in the Raman spectrum is the energy difference between the emitted photons related to the excited state of molecular vibration[9]. Theoretically, SERS enhancement primarily arises from an electromagnetic mechanism (enhancement factor of ~10^{10}–10^{11})[162], which contributes more significantly compared to the chemical enhancement mechanism (enhancement factor of 10^3)[163–165]. The electromagnetic field, generated by the activation of LSPR in plasmonic structures, enables molecules near the nanostructure's surface to absorb the near-field, then excite unique molecular vibrations. Coupling between the plasmon and molecular dipoles amplifies Raman polarizability, transmitting a far-field SERS signal of the molecule's chemical fingerprint[166]. However, the most substantial SERS

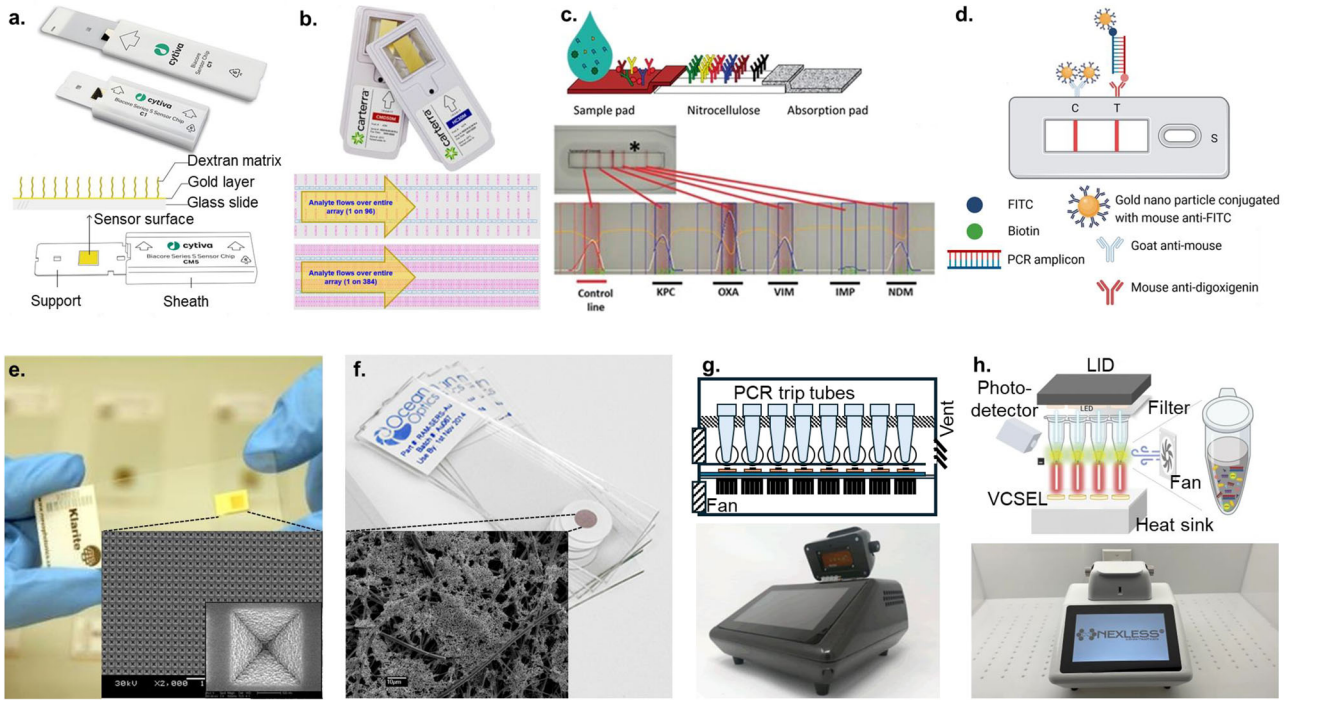

Fig. 6 | Commercial plasmonic detection platform. **a** Biacore SPR sensor chip provides real-time, ready-to-go analysis of a wide range of molecular interactions, providing kinetics, affinity, and binding data (Credit: Cytiva Life Sciences (cytiva-lifesciences.com)). **b** Carterra SPR sensors integrate with HT-SPR technology, enabling fragments and small molecules screening and antibody discovery. **c** Detection principle of NG-Test CARBA 5 Lateral Flow Assay, NG Biotech. Reprinted with permission from ref. 250. Copyright 2018 Oxford Academic. **d** Principle of detection method for Nucleic Acid Lateral Flow Immunoassay (NALFIA), Pocket Diagnostic. Reprinted with permission from ref. 254. Copyright 2024 Springer Nature. **e** Klarite SERS substrate on an array of inverted pyramid structures (credit: optics.org). Reprinted with permission from ref. 287. Copyright 2011 Applied Spectroscopy. **f** Commercial Ocean Insight SERS substrate made of gold or silver, mounted in a microscope slide. Reprinted with permission from ref. 258. Copyright 2023 Springer Nature. **g** Nanopartz Plasmonic PCR and its 8-channels for POC system (credit: Nanopartz Inc. (nanopartz.com)). **h** Nexless *P–IV* transforms is an innovative Plasmonic PCR Technology, combining advanced plasmonic gold nanorod nanoparticles with real-time quantitative PCR. (Credit: Nexless Healthcare (nexlesshealthcare.ca)).

enhancements are confined to regions extremely close to the substrate, where the intensity decreases drastically with distance (as r^{-10} for spheres). The localized areas, known as SERS hotspots, exhibit enhancement factors ranging from 10^8 to 10^{12}. They are often found at nanotips, interparticle gaps, and particle-substrate junctions[167–170]. Therefore, to increase SERS sensitivity, various hot spot-containing plasmonic optical antennas, with enhancement factors above 10^{10}, were observed in individual gold nanocrescents and nanostars with sharp edges[23,171]. Hybrid nanostructure arrays with an enhancement factor of 10^7 exhibit a detection limit down to 10^{-15} M[172,173]. The large enhancement from plasmonic nanostructures has enabled their use in real-time monitoring molecular fingerprints of biomolecules (DNA, protein, lipid, exosomes)[174–176], imaging in living cells[177], and monitoring cellular processes at the single-cell level[178]. However, in contrast, the intrinsic ultra-sensitivity of SERS can be disadvantageous for accurate quantification. This sensitivity is strongly localized within nanogaps or nanotips of nanostructures, typically 1–10 nm, where intense local electromagnetic enhancement occurs[179]. Metal colloids and nanosubstrates can be easily aggregated, contaminated, and degraded under ambient conditions[180]. Additionally, fluctuations in laser intensity and optical alignment further contribute to the signal's instability, compromising measurement reliability[181]. Moreover, SERS applications for detecting large molecules or cells, especially in complex biological matrices, remain a challenge due to the weak interaction between macromolecules and active surfaces and the low scattering cross-section of such molecules[182]. SERS also suffers from a high background noise level when the detected signal is weak, making signal extraction challenging and necessitating extensive data processing[183] or the application of AI-based analysis[184].

In this context, digital-SERS is becoming an alternative method for quantitative analysis, addressing the challenge of reduced analyte numbers, as long as a positive signal is generated[185]. Digital-SERS relies on the Poisson distribution principle, controlling the ratio between analytes and SERS substrates to ensure accurate single-molecule detection. It uses a binary detection system, "1" for positive signal and "0" for negative signal, allowing analyte numbers to be determined quantitatively[181]. While quantification at extremely low concentrations remains challenging, increasing the number of measurement events can significantly improve statistical reliability.

Plasmonic enhanced fluorescence (PEF)

Plasmonic surfaces and nanostructures have been shown to effectively enhance fluorescent reporters' intensity over 10^3 magnitudes[186–188] via locally intensified electromagnetic fields in biomolecular assays[189–192]. However, plasmonic properties of metal nanostructures affect fluorescence in two opposing ways: fluorescent emission enhancement or fluorescence quenching. Surface plasmon-quenched fluorescence occurs when a fluorophore is located within 10 nm of a plasmonic surface, leading to significant fluorescence quenching due to surface plasmon-induced resonance energy transfer from the excited state of the fluorophore to the surface plasmons of the nanoplasmonic structures[193,194]. By contrast, surface plasmon-enhanced fluorescence can occur at slightly larger distances, where the plasmonic field enhances the local electromagnetic field, increasing the fluorophore's excitation rate and radiative decay rate[194] (Fig. 5d). A metal nanocube film showed fluorescence lifetime measurements indicating fluorescence emission intensity increasing over a factor of 3 while sustaining high quantum efficiency (>0.5) and high directional emission achieving a collection efficiency of 84%[195]. A signal enhancement of nearly 3000-fold has been achieved by combining multiple factors: enhanced excitation, highly

directional light extraction, improved quantum efficiency, and suppression of blinking through modifications to the quantum dot surface[196]. Modified nanorods (fluorescence enhancers) with light emitter (molecular fluorophores), spacer layer, and recognition element (such as biotin) can enhance fluorescence emission rate by over 6700-fold compared to an 800 continuous wave (CW) fluorophore and improve the sensitivity in fluorescence-linked immunoassays by approximately 4750-fold[197]. Using recent advances in plasmonic substrates for fluorescence enhancement, personalized POC devices can overcome the major challenges to rapid, sensitive, and specific diagnosis of diseases[155,198–202]. Surface plasmon-quenched and surface plasmon-enhanced fluorescence can be combined for selective detection of nucleic acids[203–206], pathogens[200,207], and cellular internalization[208].

However, the distance sensitivity between fluorophore and metal, at which quenching and enhancement occur, is difficult to predict and control[209]. This difficulty leads to suppressed detection results and reduced signal fidelity in biosensing diagnosis. Therefore, functional spacer layers between fluorophores and metallic surfaces have been designed with precise thickness control and are now commercially available, such as atomically thin hexagonal boron nitride (h-BN)[210], polysiloxane copolymer film[211], dielectric layers[212], or polydopamine (PDA)-coated plasmonic nanocrystals[213].

Plasmonic dimer

Due to the complicated nature of designing plasmonic nanostructures for enhanced fluorescence emission, strong light-scattering plasmonic optical antennas can solve the problem corresponding to fluorophores[117]. Compared to fluorophore molecules or quantum dots, an increase in intensity of up to 10^3–10^4 can be observed in single gold nanoparticle-conjugated DNA probes coupled with target molecules[9,214,215]. The hybridization of nanoparticle probes with a single target mRNA leads to the formation of nanoparticle dimers with minimal interparticle spacing, causing a spectral peak shift resulting from strong plasmonic coupling[214] (Fig. 5e). The scattering intensity of the nanoparticle dimer was approximately 4.7-fold higher than that of the monomer[214,216]. This phenomenon allows plasmonic gold nanoparticle dimer probes to be used for quantitative imaging of target mRNA and even multiple mRNA splice isoforms in living cells, which cannot be observed by fluorophore-based probes[214]. Moreover, the enhancement factors of up to approximately 10^5 have been reported for the two-dimensional (2D) nanoparticle arrays[215,217,218].

The electromagnetic intensity in the space between two particles rises as the distance reduces from infinity to about 1 nm, resulting in a redshift of the energy mode that indicates stronger plasmonic coupling[219]. However, when the gap falls below 1 nm, the quantum tunneling of electrons across particle surfaces becomes significant, causing a notable reduction in electromagnetic field intensity[220,221]. The effectiveness of plasmonic utilization depends on selecting suitable nanoparticles, carefully controlling the nanogap for optimal coupling, and implementing molecular functionalization within the gap of the plasmonic nanoantenna[222]. Plasmonic optical antennas can be further functionalized to target biomolecules, enabling real-time tracking of molecular events[117,223,224]. This ability provides a valuable approach to investigating gene-related biological issues and diseases, including cancer, at the single-cell level.

Plasmon resonance energy transfer (PRET)

In addition to vibrational excitations, the molecular electronic fingerprint can be captured and quantified through plasmon resonance energy transfer (PRET)[225] (Fig. 5f). PRET represents the overlap between the resonance peaks of plasmon nanoparticles and the electronic resonance peaks of the biomolecule. Energy transfer likely occurs via dipole-dipole interactions between the resonating plasmon dipole in the nanoparticle and that of the biomolecule. If the plasmonic resonance energy aligns with the molecular electronic transition energy, the energy is transferred to the molecule[226]. The scattering spectrum of the nanoplasmonic optical antennas exhibits quantized quenching dips at the molecular absorption peaks (electronic transition frequency)[5,9]. Using a PRET nanosensor, plasmon quenching dips were observed to detect energy transfer in hemoglobin molecules and cytochrome C on a single nanoparticle's surface[12]. However, individual plasmonic antennas have specific spectral widths, which restrict their ability to monitor multiple types of analytes or signals. This limitation complicates broad-spectrum sensing and multiplexing detection. Current nanoparticle fabrication technologies, including printing and patterning methods, exhibit nonuniform spatial detection, which diminishes the reliability of PRET measurements, such as chemical diffusion or cellular secretion. Due to spectral and spatial limitations in PRET, continuous and comprehensive tracking is hindered, especially in complex environments like live-cell monitoring. However, metasurface-based multiplexed platforms can be precisely designed to generate specific scattering spectra by gap plasmon and grating effects to overcome the limitations in FRET spectroscopy. These metasurfaces are composed of controllable arrays of metapixels, capable of spanning the entire visible spectrum with high spatial resolution (~1.5 μm) and supporting real-time, multiplexed detection of molecular interactions over a broad field of view with distinct absorption frequencies within the visible range[227]. Moreover, PRET can be optimized over a wide spectrum, such as UV or NIR, depending on the characteristics of metallic nanoparticles that determine their plasmon resonance wavelengths in these spectral regions[228,229].

Plasmonic resonance energy transfer-based metal ion sensing (PRET-MIS)

Plasmonic resonance energy transfer-based metal ion sensing (PRET-MIS) nanospectroscopy merges metal-ligand coordination chemistry with plasmonic resonance energy transfer, resulting in enhanced sensitivity and molecular specificity at the nanoscale (Fig. 5g). This technique employs a gold nanoplasmonic probe to initiate selective energy transfer, which leads to resonant quenching in Rayleigh scattering by aligning electronic absorption bands with plasmonic resonance frequencies. Consequently, it enables accurate metal ion detection, delivering both sensitivity and selectivity through quantitative quenching that depends on the local ion concentration[230].

Quantum biological electron transfer (QBET)

The principle of quantum biological electron transfer or tunneling (QBET) is similar to the PRET method. However, by precisely controlling the function of the linker molecules as tunnel junctions for QBET detection, electron transfer can be observed in live cells and living enzymes (Fig. 5h). By using QBET spectroscopy, real-time electron transfer in the electron transport chain during cytochrome *C* dynamics was first observed at the molecular level[11]. Different optical nanostructures, such as gold nanospheres[231], gold nanorods[232], gold plant viruses[233], gold bipolar nanoelectrodes[234], plasmonic cavities[235], and pixelated metasurfaces[227], have been developed to study and modulate electron transfer dynamics in biological reactions, as well as real-time biomolecular spectroscopic imaging[236].

Reverse PRET

In contrast to PRET, reverse PRET can be intentionally employed for selective energy transfer for plasmonic quenching when molecular binding leads to a plasmonic resonance shift or intensity extinction. Owing to this phenomenon, gold nanorods functionalized with black hole quencher molecules (BHQ-3) enable real-time enzyme activity monitoring in single bacterial cells by detecting AzoR released via outer membrane vesicles, which cleaves the azo bond in BHQ-3, thereby recovering the scattering intensity of gold nanorods[13] (Fig. 5i).

Data analysis and transmission in molecular diagnostics

The COVID-19 pandemic has shifted diagnostic testing from centralized laboratories to the POC platforms. Modern standard POC diagnostics follow REASSURED criteria (real-time connectivity, ease of specimen collection, affordable, sensitive, specific, user-friendly, rapid and robust, equipment-free or simple, and deliverable to end-users)[237] to achieve high

analytical sensitivity at low concentrations of biomarkers in biological samples. Therefore, there is a need for real-time data processing and error reduction to maintain REASSURED criteria in clinical settings. With the widespread integration of automated molecular assays into portable devices, the trend has shifted towards real-time connectivity, mobile data sharing, and integration with cloud-based health systems. These systems enable data to be transmitted and analyzed in real-time for quality control and long-term monitoring of public health[238]. Moreover, integration of POC sensors with AI- and machine learning (ML)-assisted smartphone-based assays can enhance image analysis, data and signal processing, and quantitative interpretation in sensing methods such as lateral flow assays (LFAs), NAATs, and optical-based technologies[239,240]. Designed AI and deep learning algorithms can be optimized to process complex datasets and accurately recognize small changes in protein, DNA, or RNA biomarkers from exosomes[175] from multiplex or digital sensing approaches[174,184]. Moreover, convolutional neural networks (CNNs) were used as an alternative method to enhance optical-based diagnostics, offering faster and more reliable results[241].

Commercial plasmonic detection system

Recently, various commercial optical techniques integrating nanoplasmonic structures have been used for POC diagnostics, such as SPR detection, handheld SERS, and enhanced colorimetric detection in lateral flow assays[242–244].

As shown in Fig. 6a, Biacore was the first SPR-based sensor developed and is widely used for real-time, label-free analysis of molecular interactions in areas ranging from drug discovery to biotherapeutic development[245]. It is designed to qualify and quantify antibodies and proteins by evaluating their binding interactions, affinities, and kinetic profiles, from rapid association to slow dissociation rates, all while maintaining their biological function. Biacore SPR biosensors are designed with three core technologies: an optical detector system, a 50-nm layer of gold on the sensor chip, a microfluidic chip and liquid handling system[246]. Biacore systems generally achieve a LOD around 50 Da for low-molecular-weight analytes and provide various assays and monitoring capabilities to enhance the overall sensitivity of the system[246]. However, Biacore systems require careful surface chemistry optimization, and can be limited by non-specific binding in some applications. Furthermore, the system necessitates a large machine and, as a result, it tends to be quite costly. In contrast, Carterra offers a specialized high-throughput surface plasmon resonance (HT-SPR) system explicitly designed for antibody discovery and characterization (Fig. 6b). This HT-SPR technology facilitates 192 real-time interactions with molecules as small as 100 Da, utilizing the high resolution of a charge-coupled device (CCD) camera. For the kinetic and affinity measurement, HT-SPR can characterize up to 768 fragments and 1152 monoclonal antibodies (mAbs). Moreover, Carterra also develops epitope binning, which can handle interaction mapping up to 191 × 191 mAb–mAb comparisons and epitope mapping by screening up to 96 mAbs against a panel of 96 peptides. Beyond these workflows, Carterra offers flexible multiplexing, accommodating up to 192 ligands, including mutants, target variants, or controls, to meet a wide range of advanced biotherapeutic discovery and characterization needs[247]. While Carterra offers remarkably high-throughput capabilities and advanced epitope binning tools, its performance comes with trade-offs in sample consumption, system and dataset complexity, bulky instruments, and initial investment. When experiments are conducted by skilled users following SPR best practices with flexible assay design, both Biacore and Carterra platforms yield almost identical, reliable results, making them leading SPR platforms for label-free biomolecular interaction analysis and accelerating antibody library characterization toward clinical development[248]. However, in the development of POC diagnostic devices, handheld or palm-sized platforms have attracted significant attention as alternatives to bulky SPR instruments, while maintaining the capability to detect single viruses and particles smaller than 100 nm[249].

Colorimetric lateral flow assays are widely favored in POC devices for their simplicity and low cost, enabling naked-eye detection of target biomarkers. LFAs utilize gold nanoparticles for rapid testing; however, their red color restricts their applicability for multiplex assays[32]. The NG-Test CARBA 5 by NG Biotech is a multiplex lateral flow immunoassay designed using gold nanoparticles conjugated with monoclonal antibodies that are specific for the five most prevalent carbapenemase families: KPC, OXA-48-like, VIM, IMP, and NDM (Fig. 6c). All 185 carbapenemase isolates were correctly detected in less than 15 min with achieving overall 100% sensitivity and 95.3–100% specificity[250]. By a simple protocol with minimal hands-on time, no specialized instrument, and excellent sensitivity and specificity, the CARBA5-LFA has been cleared by the FDA[251] and registered in the European Database on Medical Devices (EUDAMED)[252] as an in vitro diagnostic device. Another commercial Nucleic Acid Lateral Flow Immunoassay (NALFIA) from Pocket Diagnostic is a hybrid detection method combining nucleic acid amplification with LFA for visual detection of target DNA/RNA sequences (Fig. 6d). The target sequence is amplified initially with a fluorophore-labeled primer (biotin, fluorescein (FAM) or digoxigenin), then introduced onto the lateral flow strip, where it binds to nanoparticle-conjugated antibodies, producing a visible color change[253]. NALFIA obtains high sensitivity and specificity, comparable to real-time PCR[254]; however, it still suffers from quantitative accuracy, sensitivity and specificity at lower concentrations, and multiplexing capacity.

Highly scalable SERS sensors have emerged as the next generation in molecular detection due to their high sensitivity, noninvasiveness, and multiplex capability[164,255]. The commercially available Klarite substrate was fabricated using photolithography techniques on a silicon wafer (Fig. 6e) to fabricate an inverted pyramid array of hot spots with highly reproducibility and uniformity[256]. Under ideal conditions, these substrates obtain a typical relative standard deviation (RSD) from 10 to 15% under drop-and-dry conditions, with low substrate background[257]. Another ready-to-use SERS substrate from Ocean Insight is designed for rapid and sensitive detection of chemicals and biomolecules (Fig. 6f). The SERS active areas (5.5 mm diameter circle) are typically made of gold (excitation wavelength of 785 nm) or silver (excitation wavelength of 532 nm), offer reliable performance, and can be easily integrated with a handheld Raman spectrometer. A comparison of the LOD for three commercial SERS substrates from Hamamatsu, SERSitive, and Ocean Insight shows that at a 10^{-6} M concentration, SERSitive and Ocean Insight offer better performance. However, background noise limits their effectiveness at lower concentrations. However, at 10^{-8} M, the Hamamatsu substrate demonstrates higher sensitivity for thiophenol detection, especially at 633 nm excitation[258]. Although the commercial SERS substrates are well recognized, their practical applications remain challenges, including low reproducibility, small active surface areas, batch-to-batch variation, and high manufacturing costs.

Apart from direct virus capture, nucleic acid amplification plays a vital role in POC diagnostics. As illustrated in Fig. 6g, the photonic PCR platform developed by Nanopartz utilizes gold nanoparticles and gold nanorods in the PCR reaction mixtures.These particles rapidly convert light to heat, with over 90% absorption and 100% efficiency, achieving heating rates of up to 20 °C/s[259]. The Nanopartz photonic PCR prototype is simple, fast, offering thermocycling capability and highly specific amplification. Moreover, it is fully compatible with standard PCR protocols, making it a promising candidate for the integrating plasmonic and conventional PCR into a self-powered, portable POC device. The ultra-fast Nexless Kimera P-IV plasmonic RT-qPCR technology integrates gold nanorods and vertical surface-emitting lasers to replace conventional heating methods like Peltier blocks. This approach enables rapid thermal cycling and achieves a PCR efficiency of 88.3% in under 10 min (Fig. 6h). The device can detect as few as 1 DNA copy with 100% accuracy in direct-urine analysis[260]. However, to achieve reliable results, careful biological reagents preparation - such as primer designs - is needed, and further clinical validation is still required.

Future perspectives and challenges

While nanoplasmonics-based actuators for the selective trapping and enrichment of biological samples and biosensors for the sensitive detection of protein, RNA, and DNA biomarkers hold the promise of revolutionizing biomedical diagnostics, several challenges—including fabrication scalability, stability, and specificity—must be addressed to fully realize their potential for clinical applications.

Scalability and cost-effectiveness

The fabrication of highly organized and reproducible nanostructures continues to represent one of the principal challenges in the area of nanoplasmonics-based biosensors.

The prevailing top-down fabrication methods for laboratory-scale applications with resolution of 100 nm or better, including electron beam lithography (EBL) and focused ion beam (FIB) lithography, are characterized by high precision; however, they are also time-intensive, costly, and lack the scalability necessary for mass production. This scenario has engendered a demand for low-cost alternative manufacturing methods to facilitate commercialization.

In this context, large-scale and cost-effective top-down lithography techniques, such as nanoimprinting, nanostencils, interference lithography, and deep and extreme ultraviolet lithography, have emerged as viable alternative manufacturing strategies[261,262]. Attainment of uniformity and high throughput remains a critical concern. Low-cost, disposable biosensor chips are preferred to prevent cross-contamination and eliminate the need for complex cleaning processes when working with biological samples. Therefore, systems that support single-use cartridges paired with a standalone reader represent the most practical solution. However, intensive research is necessary to address challenges in fabrication methods as well as the cost of biomaterials (e.g., reagents) required to manufacture inexpensive single-use cartridges[263].

Complex biological sample handling

The extensive range of analytes and matrix compositions—such as bodily fluids in medical diagnostics and food samples in food safety—presents distinct challenges for sample collection and processing, which are essential for on-site biosensing. Microfluidic systems demonstrate significant utility in biosensor integration by facilitating multiplexed functions such as sample preparation, concentration, and analyte transport, while simultaneously minimizing the volume of required samples and limiting the utilization of expensive reagents[264–266]. Furthermore, the nanoplasmonic actuators enhance purification and selectively enrich targeted biomarkers. Nanoplasmonic sensors can be integrated with nanoplasmonic actuators into a smart integrated photonics and microfluidic integrated circuit (IC) system, which can be employed for sample preparation, as previously discussed, and holds promise for integration with microfluidics. This combination aims to achieve high specificity and sensitivity in the detection of specific biomolecules within complex samples. However, several challenges remain that hinder the advancement of technology transfer and commercialization, primarily due to the complexities such as material compatibility, alignment precision, and fluidic control that are involved in integrating all components into a single, portable platform[265]. In addition, efficiently transferring light from an external source to the plasmonic structure within the microfluidic channel without significant loss requires clear optical paths that can be obstructed by microfluidic materials or channel designs.

Surface chemistry for biofunctionalization

While sensitivity, resolution, and detection speed represent crucial metrics for the assessment of nanoplasmonic biosensor performance, surface chemistry plays a vital role in determining the efficacy of biosensing through molecular recognition between receptors and targets. Thus, it is imperative that the surface chemistry of nanoplasmonic sensors is both robust and reliable to facilitate effective biofunctionalization, ensuring stable binding of biomolecules such as antibodies or aptamers. However, the nonplanar and heterogeneous characteristics of nanoplasmonic surfaces pose significant challenges for surface modification.

Nanoplasmonic surfaces, which often include three-dimensional or non-planar nanostructures such as nanoholes, nanopillars, or nanoparticles and may incorporate multiple materials, present greater challenges for uniform biofunctionalization compared to flat surfaces. This complexity necessitates the implementation of innovative approaches, such as material-selective or site-specific functionalization techniques.

Moreover, integrating nanoplasmonic sensors with biomembranes allows for the incorporation of membrane-bound receptors and mitigates nonspecific binding by passivating the sensor surface[267]. Furthermore, a notable lack of analytical methods capable of adequately evaluating and quantifying each step of functionalization persists, a gap that is crucial for assessing the diffusion of these sensors within the market[263].

Emerging directions

Advancements in materials science and optical physics are anticipated to facilitate further progress in nanoplasmonic biosensors. Recently, 2D materials such as graphene, transition metal dichalcogenides (TMDs), and black phosphorus have been utilized with increasing frequency in nanoplasmonic biosensing, owing to their distinctive properties, thereby playing a crucial role in the detection of various biomolecules[268]. Low-dimensional van der Waals (vdW) materials provide distinct advantages for nanophotonic biosensing by generating highly confined polaritonic waves. Their diminished dimensionality—illustrated by two-dimensional graphene—augments plasmonic field confinement, leading to enhanced sensitivity and performance compared to conventional nanophotonic systems reliant on surface plasmons in metallic films[269]. Various biosensing techniques, including SPR[270], FRET, and evanescent wave-based methods, along with the associated characteristics, synthesis approaches, and integration techniques of two-dimensional materials, have attracted significant attention. Alternative materials capable of generating plasmonically enhanced light–matter interactions have garnered considerable interest, particularly copper, aluminum, indium, and magnesium, as they present a cost-effective substitute for conventional metals such as gold and silver in large-scale applications[271]. Integrating microfluidics[14], flexible electronics[272], and wireless communication[273] will facilitate the development of compact, portable, and user-friendly POC devices. Furthermore, the incorporation of AI[274] and ML for real-time data analysis and interpretation will substantially enhance diagnostic accuracy, providing label-free, multiplexed detection at ultra-low concentrations. Through sustained interdisciplinary collaboration, nanoplasmonic biosensors hold the potential to transform healthcare, environmental monitoring, and biosecurity by means of rapid, reliable, and accessible sensing technologies.

Conclusion and outlook

In this review, we examine the advancements in nanoplasmonic optical antennas utilized as biosensors and actuators within the realm of molecular diagnostics. Integrated nanoplasmonic biosensors have the potential to optimize the sample preparation process while inflicting minimal damage through plasmonic trapping. Moreover, they facilitate label-free, real-time detection of a singular target through plasmonic photothermal actuation for the purposes of sample enrichment and lysis. Recent advancements in integrated molecular diagnostic systems utilizing nanoplasmonics demonstrate high sensitivity, rapid response times, and portability for disease detection through the application of the plasmonic photothermal effect in NAATs, rendering them particularly beneficial in resource-limited settings. Smartphones equipped with integrated detection systems utilizing plasmonic biosensors and sample preparation platforms will establish an efficient molecular diagnostic system. This system amalgamates sample enrichment, lysis, amplification, and detection processes onto a singular chip. Such systems represent promising instruments for remote healthcare and personalized health monitoring. Furthermore, nanoplasmonic optical antennas as actuators and biosensors exhibit substantial potential not only for advanced real-time healthcare tracking and monitoring but also for elucidating life sciences and quantum biology at the single-cell level. For instance, nanoplasmonics serve to illustrate intracellular quantum processes, such as electron transfer in mitochondria[11] and bacterial communication[13] with one another as well as with host cells, thereby illuminating the field of quantum biology. Furthermore, the cavity quantum electrodynamic properties stemming from the strong light-matter interaction between surface plasmons and emitters-whether they be fluorescent probe-tagged proteins or biomolecular emitters such as chlorophyll[275,276],

can be a promising quantum plasmonic biosensor platform that does not necessitate sophisticated measurement tools or cryogenic temperatures. Additionally, alternative plasmonic materials, such as graphene derivatives, may be integrated into biosensor systems[277]. Nanoplasmonic optical antennas are utilized in high-speed hyperspectral imaging systems to observe and analyze biomolecular interactions within living biological cells at a single-copy resolution. Future advancements in nanoplasmonics are expected to transition from research to practical healthcare applications, thereby fostering innovative diagnostics and personalized medicine.

Data availability

No datasets were generated or analysed during the current study.

Received: 24 January 2025; Accepted: 7 July 2025;
Published online: 08 December 2025

References

1. Marchenko, V. Y. et al. Characterization of H5N1 avian influenza virus isolated from bird in Russia with the E627K mutation in the PB2 protein. *Sci. Rep.* **14**, 26490 (2024).
2. Qun, L. et al. Early Transmission Dynamics in Wuhan, China, of Novel Coronavirus–Infected Pneumonia. *N. Engl. J. Med.* **382**, 1199–1207 (2020).
3. Burki, T. Outbreak of coronavirus disease 2019. *Lancet Infect. Dis.* **20**, 292–293 (2020).
4. Novotny, L. & Van Hulst, N. Antennas for light. *Nat. Photonics* **5**, 83–90 (2011).
5. Liu, W., Chung, K., Yu, S. & Lee, L. P. Nanoplasmonic biosensors for environmental sustainability and human health. *Chem. Soc. Rev.* **53**, 10491–10522 (2024).
6. Islam, M. M. & Koirala, D. Toward a next-generation diagnostic tool: A review on emerging isothermal nucleic acid amplification techniques for the detection of SARS-CoV-2 and other infectious viruses. *Anal. Chim. Acta* **1209**, 339338 (2022).
7. Yu, E. S. et al. Highly Efficient On-Chip Photothermal Cell Lysis for Nucleic Acid Extraction Using Localized Plasmonic Heating of Strongly Absorbing Au Nanoislands. *ACS Appl Mater. Interfaces* **15**, 34323–34331 (2023).
8. Cho, B. et al. Nanophotonic Cell Lysis and Polymerase Chain Reaction with Gravity-Driven Cell Enrichment for Rapid Detection of Pathogens. *ACS Nano* **13**, 13866–13874 (2019).
9. Xin, H., Namgung, B. & Lee, L. P. Nanoplasmonic optical antennas for life sciences and medicine. *Nat. Rev. Mater.* **3**, 228–243 (2018).
10. Kneipp, J., Kneipp, H. & Kneipp, K. SERS—a single-molecule and nanoscale tool for bioanalytics. *Chem. Soc. Rev.* **37**, 1052–1060 (2008).
11. Xin, H. et al. Quantum biological tunnel junction for electron transfer imaging in live cells. *Nat. Commun.* **10**, 3245 (2019).
12. Liu, G. L., Long, Y.-T., Choi, Y., Kang, T. & Lee, L. P. Quantized plasmon quenching dips nanospectroscopy via plasmon resonance energy transfer. *Nat. Methods* **4**, 1015–1017 (2007).
13. Lu, D. et al. Dynamic monitoring of oscillatory enzyme activity of individual live bacteria via nanoplasmonic optical antennas. *Nat. Photonics* **17**, 904–911 (2023).
14. AbdElFatah, T. et al. Nanoplasmonic amplification in microfluidics enables accelerated colorimetric quantification of nucleic acid biomarkers from pathogens. *Nat. Nanotechnol.* **18**, 922–932 (2023).
15. Nakatsuji, H. et al. Thermosensitive Ion Channel Activation in Single Neuronal Cells by Using Surface-Engineered Plasmonic Nanoparticles. *Angew. Chem. Int. Ed.* **54**, 11725–11729 (2015).
16. Jain, P. K., Lee, K. S., El-Sayed, I. H. & El-Sayed, M. A. Calculated absorption and scattering properties of gold nanoparticles of different size, shape, and composition: Applications in biological imaging and biomedicine. *J. Phys. Chem. B* **110**, 7238–7248 (2006).
17. Turkevich, J., Stevenson, P. C. & Hillier, J. A study of the nucleation and growth processes in the synthesis of colloidal gold. *Discuss Faraday Soc.* **11**, 55–75 (1951).
18. Yu, Y. Y., Chang, S. S., Lee, C. L. & Wang, C. C. Gold Nanorods: Electrochemical Synthesis and Optical Properties. *J. Phys. Chem. B* **101**, 6661–6664 (1997).
19. Oldenburg, S. J., Averitt, R. D., Westcott, S. L. & Halas, N. J. Nanoengineering of optical resonances. *Chem. Phys. Lett.* **288**, 243–247 (1998).
20. Sun, Y. & Xia, Y. Shape-Controlled Synthesis of Gold and Silver Nanoparticles. *Science ((1979))* **298**, 2176–2179 (2002).
21. Charnay, C. et al. Reduced symmetry metallodielectric nanoparticles: chemical synthesis and plasmonic properties. *J. Phys. Chem. B* **107**, 7327–7333 (2003).
22. Nehl, C. L., Liao, H. & Hafner, J. H. Optical properties of star-shaped gold nanoparticles. *Nano Lett.* **6**, 683–688 (2006).
23. Lu, Y., Liu, G. L., Kim, J., Mejia, Y. X. & Lee, L. P. Nanophotonic crescent moon structures with sharp edge for ultrasensitive biomolecular detection by local electromagnetic field enhancement effect. *Nano Lett.* **5**, 119–124 (2005).
24. Bukasov, R. & Shumaker-Parry, J. S. Highly tunable infrared extinction properties of gold nanocrescents. *Nano Lett.* **7**, 1113–1118 (2007).
25. Liu, G. L., Lu, Y., Kim, J., Doll, J. C. & Lee, L. P. Magnetic nanocrescents as controllable surface-enhanced Raman scattering nanoprobes for biomolecular imaging. *Adv. Mater.* **17**, 2683–2688 (2005).
26. Li, D., Zhang, Q., Xing, L. & Chen, B. Theoretical and in vivo experimental investigation of laser hyperthermia for vascular dermatology mediated by liposome@Au core–shell nanoparticles. *Lasers Med. Sci.* **37**, 3269–3277 (2022).
27. Bhaskar, S. & Lim, S. Engineering protein nanocages as carriers for biomedical applications. *NPG Asia Mater.* **9**, e371–e371 (2017).
28. Xia, Y. et al. Gold nanocages: from synthesis to theranostic applications. *Acc. Chem. Res.* **44**, 914–924 (2011).
29. Wang, T. et al. Multifunctional hollow mesoporous silica nanocages for cancer cell detection and the combined chemotherapy and photodynamic therapy. *ACS Appl. Mater. Interfaces* **3**, 2479–2486 (2011).
30. Chen, J. et al. Gold nanocages as photothermal transducers for cancer treatment. *Small* **6**, 811–817 (2010).
31. Kim, H., Chung, K., Lee, S., Kim, D. H. & Lee, H. Near-infrared light-responsive nanomaterials for cancer theranostics. *WIREs Nanomed. Nanobiotechnol.* **8**, 23–45 (2016).
32. Shin, M. et al. Highly sensitive multiplexed colorimetric lateral flow immunoassay by plasmon-controlled metal–silica isoform nanocomposites: PINs. *Nano Converg.* **11**, 42 (2024).
33. Li, H. et al. Optical pulling forces and their applications. *Adv. Opt. Photonics* **12**, 288–366 (2020).
34. Bradac, C. Nanoscale optical trapping: a review. *Adv. Opt. Mater.* **6**, 1800005 (2018).
35. Xin, H. et al. Optical forces: from fundamental to biological applications. *Adv. Mater.* **32**, 2001994 (2020).
36. Juan, M. L., Righini, M. & Quidant, R. Plasmon nano-optical tweezers. *Nat. Photonics* **5**, 349–356 (2011).
37. Maragò, O. M., Jones, P. H., Gucciardi, P. G., Volpe, G. & Ferrari, A. C. Optical trapping and manipulation of nanostructures. *Nat. Nanotechnol.* **8**, 807–819 (2013).
38. Polimeno, P. et al. Optical tweezers and their applications. *J. Quant. Spectrosc. Radiat. Transf.* **218**, 131–150 (2018).
39. Dholakia, K. & Zemánek, P. Colloquium: gripped by light: optical binding. *Rev. Mod. Phys.* **82**, 1767–1791 (2010).
40. Maier, S. *Plasmonics: Fundamentals and Applications*. (Springer, New York, 2007).

41. Tan, H., Hu, H., Huang, L. & Qian, K. Plasmonic tweezers for optical manipulation and biomedical applications. *Analyst* **145**, 5699–5712 (2020).
42. Quidant, R. & Girard, C. Surface-plasmon-based optical manipulation. *Laser Photon Rev.* **2**, 47–57 (2008).
43. Messina, E. et al. Plasmon-enhanced optical trapping of gold nanoaggregates with selected optical properties. *ACS Nano* **5**, 905–913 (2011).
44. Ploschner, M., Čižmár, T., Mazilu, M., Di Falco, A. & Dholakia, K. Bidirectional optical sorting of gold nanoparticles. *Nano Lett.* **12**, 1923–1927 (2012).
45. Quidant, R., Petrov, D. & Badenes, G. Radiation forces on a Rayleigh dielectric sphere in a patterned optical near field. *Opt. Lett.* **30**, 1009–1011 (2005).
46. Verschueren, D. V. et al. Label-Free Optical Detection of DNA Translocations through Plasmonic Nanopores. *ACS Nano* **13**, 61–70 (2019).
47. Righini, M. et al. Nano-optical trapping of Rayleigh particles and Escherichia coli bacteria with resonant optical antennas. *Nano Lett.* **9**, 3387–3391 (2009).
48. Yoon, S. J. et al. Non-fluorescent nanoscopic monitoring of a single trapped nanoparticle via nonlinear point sources. *Nat. Commun.* **9**, 2218 (2018).
49. Tanaka, Y., Kaneda, S. & Sasaki, K. Nanostructured potential of optical trapping using a plasmonic nanoblock pair. *Nano Lett.* **13**, 2146–2150 (2013).
50. Jones, S., Andrén, D., Karpinski, P. & Käll, M. Photothermal heating of plasmonic nanoantennas: influence on trapped particle dynamics and colloid distribution. *ACS Photonics* **5**, 2878–2887 (2018).
51. Shoji, T. et al. Permanent fixing or reversible trapping and release of DNA micropatterns on a gold nanostructure using continuous-wave or femtosecond-pulsed near-infrared laser light. *J. Am. Chem. Soc.* **135**, 6643–6648 (2013).
52. Jiang, Q., Rogez, B., Claude, J.-B., Baffou, G. & Wenger, J. Temperature measurement in plasmonic nanoapertures used for optical trapping. *ACS Photonics* **6**, 1763–1773 (2019).
53. Xu, Z., Song, W. & Crozier, K. B. Direct particle tracking observation and Brownian dynamics simulations of a single nanoparticle optically trapped by a plasmonic nanoaperture. *ACS Photonics* **5**, 2850–2859 (2018).
54. Belkin, M., Chao, S.-H., Jonsson, M. P., Dekker, C. & Aksimentiev, A. Plasmonic nanopores for trapping, controlling displacement, and sequencing of DNA. *ACS Nano* **9**, 10598–10611 (2015).
55. Zhang, Y. et al. Plasmonic tweezers: for nanoscale optical trapping and beyond. *Light Sci. Appl* **10**, 59 (2021).
56. Renkes, S. et al. Self-induced back-action actuated nanopore electrophoresis (SANE) sensing. in *Single Molecule Sensing Beyond Fluorescence* (eds Bowen, W., Vollmer, F. & Gordon, R.) 389–412 (Springer International Publishing, Cham, 2022).
57. Asadzadeh, H., Renkes, S., Kim, M. & Alexandrakis, G. Multi-physics simulations and experimental comparisons for the optical and electrical forces acting on a silica nanoparticle trapped by a double-nanohole plasmonic nanopore sensor. *Sens. Biosens. Res* **41**, 100581 (2023).
58. Asadzadeh, H., Renkes, S., Kim, M. & Alexandrakis, G. Computational and experimental study of AC measurements performed by a double-nanohole plasmonic nanopore sensor on 20 nm silica nanoparticles. *Sens. Biosens. Res.* **46**, 100694 (2024).
59. Xu, Z., Song, W. & Crozier, K. B. Optical trapping of nanoparticles using all-silicon nanoantennas. *ACS Photonics* **5**, 4993–5001 (2018).
60. Ndukaife, J. C. et al. Long-range and rapid transport of individual nano-objects by a hybrid electrothermoplasmonic nanotweezer. *Nat. Nanotechnol.* **11**, 53–59 (2016).
61. Garcia-Guirado, J. et al. Overcoming Diffusion-Limited Biosensing by Electrothermoplasmonics. *ACS Photonics* **5**, 3673–3679 (2018).
62. Hong, C. & Ndukaife, J. C. Scalable trapping of single nanosized extracellular vesicles using plasmonics. *Nat. Commun.* **14**, 4801 (2023).
63. Li, T. et al. Virus detection light diffraction fingerprints for biological applications. *Sci. Adv.* **10**, eadl3466 (2024).
64. Bergeron, J., Zehtabi-Oskuie, A., Ghaffari, S., Pang, Y. & Gordon, R. Optical trapping of nanoparticles. *J. Vis. Exp.* **71**, e4424 (2013).
65. Xiong, J. et al. Wake-riding effect-inspired opto-hydrodynamic diatombot for non-invasive trapping and removal of nano-biothreats. *Adv. Sci.* **10**, 2301365 (2023).
66. Li, X. et al. Opto-hydrodynamic driven 3D dynamic microswarm petals. *Laser Photon Rev.* **18**, 2300480 (2024).
67. Shi, Y. et al. Light-induced cold Marangoni flow for microswarm actuation: from intelligent behaviors to collective drug delivery. *Laser Photon Rev.* **16**, 2200533 (2022).
68. He, Z. et al. Opto-thermal-tension mediated precision large-scale particle manipulation and flexible patterning. *Adv. Sci.* **11**, 2405211 (2024).
69. Shi, Y. et al. Adaptive opto-thermal-hydrodynamic manipulation and polymerization (AOTHMAP) for 4D colloidal patterning. *Adv. Mater.* **36**, 2412895 (2024).
70. Park, J. et al. Colloidal multiscale assembly via photothermally driven convective flow for sensitive in-solution plasmonic detections. *Small* **18**, 2201075 (2022).
71. Setoura, K., Tsuji, T., Ito, S., Kawano, S. & Miyasaka, H. Opto-thermophoretic separation and trapping of plasmonic nanoparticles. *Nanoscale* **11**, 21093–21102 (2019).
72. Andrén, D. et al. Probing photothermal effects on optically trapped gold nanorods by simultaneous plasmon spectroscopy and Brownian dynamics analysis. *ACS Nano* **11**, 10053–10061 (2017).
73. Jiang, Q., Rogez, B., Claude, J. B., Baffou, G. & Wenger, J. Quantifying the role of the surfactant and the thermophoretic force in plasmonic nano-optical trapping. *Nano Lett.* **20**, 8811–8817 (2020).
74. Li, J. et al. Opto-refrigerative tweezers. *Sci. Adv.* **7**, eabh1101 (2021).
75. Lin, L. et al. Thermophoretic tweezers for low-power and versatile manipulation of biological cells. *ACS Nano* **11**, 3147–3154 (2017).
76. Liu, C. et al. Low-cost thermophoretic profiling of extracellular-vesicle surface proteins for the early detection and classification of cancers. *Nat. Biomed. Eng.* **3**, 183–193 (2019).
77. Shoji, T. et al. Plasmonic manipulation of DNA using a combination of optical and thermophoretic forces: separation of different-sized DNA from mixture solution. *Sci. Rep.* **10**, 3349 (2020).
78. Kollipara, P. S. et al. Hypothermal opto-thermophoretic tweezers. *Nat. Commun.* **14**, 5133 (2023).
79. Kim, J. A., Yeatman, E. M. & Thompson, A. J. Plasmonic optical fiber for bacteria manipulation—characterization and visualization of accumulation behavior under plasmo-thermal trapping. *Biomed. Opt. Express* **12**, 3917 (2021).
80. Crozier, K. B. Plasmonic nanotweezers: what's next?. *ACS Photonics* **11**, 321–333 (2024).
81. Ayari, S., Dussault, D., Millette, M., Hamdi, M. & Lacroix, M. Response of *Bacillus cereus* to γ-irradiation in combination with Carvacrol or mild heat treatment. *J. Agric Food Chem.* **58**, 8217–8224 (2010).
82. Smyrlaki, I. et al. Massive and rapid COVID-19 testing is feasible by extraction-free SARS-CoV-2 RT-PCR. *Nat. Commun.* **11**, 1–12 (2020).
83. Li, H. & Gänzle, M. Some like it hot: heat resistance of *Escherichia coli* in food. *Front. Microbiol.* **7**, 1763 (2016).
84. Tang, J. W. The effect of environmental parameters on the survival of airborne infectious agents. *J. R. Soc. Interface* **6**, S737–S746 (2009).

85. Baffou, G., Cichos, F. & Quidant, R. Applications and challenges of thermoplasmonics. *Nat. Mater.* **19**, 946–958 (2020).
86. Mbeh, D. A. et al. Human alveolar epithelial cell responses to core-shell superparamagnetic iron oxide nanoparticles (spions). *Langmuir* **31**, 3829–3839 (2015).
87. Slavin, Y. N., Asnis, J., Häfeli, U. O. & Bach, H. Metal nanoparticles: understanding the mechanisms behind antibacterial activity. *J. Nanobiotechnol.***15**, 65 (2017).
88. Hayden, S. C. et al. Aggregation and interaction of cationic nanoparticles on bacterial surfaces. *J. Am. Chem. Soc.* **134**, 6920–6923 (2012).
89. Joo, S. H. & Aggarwal, S. Factors impacting the interactions of engineered nanoparticles with bacterial cells and biofilms: Mechanistic insights and state of knowledge. *J. Environ. Manag.* **225**, 62–74 (2018).
90. Baffou, G. & Quidant, R. Thermo-plasmonics: using metallic nanostructures as nano-sources of heat. *Laser Photon Rev.* **7**, 171–187 (2013).
91. Loo, C. et al. Nanoshell-Enabled Photonics-Based Imaging and Therapy of Cancer. *Technol. Cancer Res Treat.* **3**, 33–40 (2004).
92. Skrabalak, S. E., Au, L., Li, X. & Xia, Y. Facile synthesis of Ag nanocubes and Au nanocages. *Nat. Protoc.* **2**, 2182–2190 (2007).
93. Huang, X., El-Sayed, I. H., Qian, W. & El-Sayed, M. A. Cancer cell imaging and photothermal therapy in the near-infrared region by using gold nanorods. *J. Am. Chem. Soc.* **128**, 2115–2120 (2006).
94. Cao, L., Barsic, D. N., Guichard, A. R. & Brongersma, M. L. Plasmon-assisted local temperature control to pattern individual semiconductor nanowires and carbon nanotubes. *Nano Lett.* **7**, 3523–3527 (2007).
95. Lukianova-Hleb, E. Y., Anderson, L. J. E., Lee, S., Hafner, J. H. & Lapotko, D. O. Hot plasmonic interactions: a new look at the photothermal efficacy of gold nanoparticles. *Phys. Chem. Chem. Phys.* **12**, 12237–12244 (2010).
96. Diallo, A. T., Tlemçani, M., Khan, M., Spadavecchia, J. & Djaker, N. Size, shape, and wavelength effect on photothermal heat elevation of gold nanoparticles: absorption coefficient experimental measurement. *Part. Part. Syst. Charact.* **37**, 2000255 (2020).
97. Baffou, G., Quidant, R. & García de Abajo, F. J. Nanoscale control of optical heating in complex plasmonic systems. *ACS Nano* **4**, 709–716 (2010).
98. Kwon, K. et al. Continuous adsorption and photothermal lysis of airborne bacteria using a gold-nanoparticle-embedded-geometrically activated surface interaction (gold-GASI) chip. *Sens. Actuators B Chem.* **248**, 580–588 (2017).
99. Kwon, K., Gwak, H., Hyun, K.-A., Kwak, B.-S. & Jung, H.-I. High-throughput microfluidic chip for magnetic enrichment and photothermal DNA extraction of foodborne bacteria. *Sens. Actuators B Chem.* **294**, 62–68 (2019).
100. Cheong, K. H. et al. Gold nanoparticles for one step DNA extraction and real-time PCR of pathogens in a single chamber. *Lab Chip* **8**, 810–813 (2008).
101. Lee, J.-H. et al. Nanoplasmonic rapid antimicrobial-resistance point-of-care identification device: RAPIDx. *Adv. Health. Mater.* **14**, 2402044 (2025).
102. Phakatkar, A. H. et al. In situ microscopic studies on the interaction of multi-principal element nanoparticles and bacteria. *ACS Nano* **17**, 5880–5893 (2023).
103. Cao, X. et al. Template-free preparation of hollow Sb2S3 microspheres as supports for Ag nanoparticles and photocatalytic properties of the constructed metal-semiconductor nanostructures. *Adv. Funct. Mater.* **16**, 896–902 (2006).
104. Virkutyte, J. & Varma, R. S. Fabrication and visible light photocatalytic activity of a novel Ag/TiO2-xNx nanocatalyst. *N. J. Chem.* **34**, 1094–1096 (2010).
105. Duchene, J. S. et al. Prolonged hot electron dynamics in plasmonic-metal/semiconductor heterostructures with implications for solar photocatalysis. *Angew. Chem. Int. Ed.* **53**, 7887–7891 (2014).
106. Li, J. et al. Interfacial engineering of Bi2S3/Ti3C2Tx MXene based on work function for rapid photo-excited bacteria-killing. *Nat. Commun.* **12**, 1224 (2021).
107. Cui, Z., Zhang, L., Wang, Y. & He, W. Plasmon excitation facilitating generation of electrons and reactive oxygen species for broad spectrum photocatalytic activity. *Appl. Surf. Sci.* **584**, 152655 (2022).
108. Fu, P. P., Xia, Q., Hwang, H.-M., Ray, P. C. & Yu, H. Mechanisms of nanotoxicity: generation of reactive oxygen species. *J. Food Drug Anal.* **22**, 64–75 (2014).
109. Yu, Z. et al. Reactive oxygen species-related nanoparticle toxicity in the biomedical field. *Nanoscale Res. Lett.* **15**, 115 (2020).
110. Dubi, Y. & Sivan, Y. "Hot" electrons in metallic nanostructures—non-thermal carriers or heating?. *Light Sci. Appl.* **8**, 89 (2019).
111. Jeong, J., Shin, H. H. & Kim, Z. H. Unveiling the mechanism of plasmon photocatalysis via multiquantum vibrational excitation. *ACS Nano* **18**, 25290–25301 (2024).
112. Linic, S., Aslam, U., Boerigter, C. & Morabito, M. Photochemical transformations on plasmonic metal nanoparticles. *Nat. Mater.* **14**, 567–576 (2015).
113. Block, A. et al. Tracking ultrafast hot-electron diffusion in space and time by ultrafast thermomodulation microscopy. *Sci. Adv.* **5**, eaav8965 (2019).
114. Zhan, C. et al. Plasmon-mediated chemical reactions. *Nat. Rev. Methods Prim.* **3**, 12 (2023).
115. Del Fatti, N. et al. Nonequilibrium electron dynamics in noble metals. *Phys. Rev. B* **61**, 16956–16966 (2000).
116. Zhang, C., Jia, F., Li, Z., Huang, X. & Lu, G. Plasmon-generated hot holes for chemical reactions. *Nano Res.* **13**, 3183–3197 (2020).
117. Cognet, L. et al. Single metallic nanoparticle imaging for protein detection in cells. *Proc. Natl Acad. Sci. USA* **100**, 11350–11355 (2003).
118. Sun, C.-K., Vallée, F., Acioli, L. H., Ippen, E. P. & Fujimoto, J. G. Femtosecond-tunable measurement of electron thermalization in gold. *Phys. Rev. B* **50**, 15337–15348 (1994).
119. Blumenfeld, N. R. et al. Multiplexed reverse-transcriptase quantitative polymerase chain reaction using plasmonic nanoparticles for point-of-care COVID-19 diagnosis. *Nat. Nanotechnol.* **17**, 984–992 (2022).
120. Jiang, K. et al. Plasmonic colorimetric PCR for rapid molecular diagnostic assays. *Sens. Actuators B Chem.* **337**, 129762 (2021).
121. Li, M., Lin, Y. C., Wu, C. C. & Liu, H. S. Enhancing the efficiency of a PCR using gold nanoparticles. *Nucleic Acids Res.* **33**, e184 (2005).
122. Roche, P. J. R. et al. Demonstration of a plasmonic thermocycler for the amplification of human androgen receptor DNA. *Analyst* **137**, 4475–4481 (2012).
123. Roche, P. J. R. et al. Real time plasmonic qPCR: how fast is ultra-fast? 30 cycles in 54 seconds. *Analyst* **142**, 1746–1755 (2017).
124. Cheong, J. et al. Fast detection of SARS-CoV-2 RNA via the integration of plasmonic thermocycling and fluorescence detection in a portable device. *Nat. Biomed. Eng.* **4**, 1159–1167 (2020).
125. Kim, K. H. et al. Ultra-fast photonic digital polymerase chain reaction based on N-heterocyclic carbene self-assembled monolayer. *Adv. Funct. Mater.* **33**, 2303728 (2023).
126. Son, J. H. et al. Rapid optical cavity PCR. *Adv. Health. Mater.* **5**, 167–174 (2016).
127. Lee, Y. et al. Nanoplasmonic on-chip PCR for rapid precision molecular diagnostics. *ACS Appl Mater. Interfaces* **12**, 12533–12540 (2020).
128. Kang, B. H. et al. Ultrafast and real-time nanoplasmonic on-chip polymerase chain reaction for rapid and quantitative molecular diagnostics. *ACS Nano* **15**, 10194–10202 (2021).

129. Jiang, K. et al. Plasmonic cross-linking colorimetric PCR for simple and sensitive nucleic acid detection. *Nano Lett.* **23**, 3897–3903 (2023).
130. Lillis, L. et al. Factors influencing recombinase polymerase amplification (RPA) assay outcomes at point of care. *Mol. Cell Probes* **30**, 74–78 (2016).
131. Warmt, C., Yaslanmaz, C. & Henkel, J. Investigation and validation of labelling loop mediated isothermal amplification (LAMP) products with different nucleotide modifications for various downstream analysis. *Sci. Rep.* **12**, 7137 (2022).
132. Lin, Q. et al. A smart single-loop-mediated isothermal amplification facilitates flexible SNP probe design for on-site rapid differentiation of SARS-CoV-2 omicron variants. *Adv. Sci.* **12**, 2502708 (2025).
133. Oliveira, B. B., Veigas, B. & Baptista, P. V. Isothermal amplification of nucleic acids: the race for the Next "Gold Standard". *Front. Sens.* **2**, 752600 (2021).
134. Kim, J. U. et al. Omnidirectional, broadband light absorption in a hierarchical nanoturf membrane for an advanced solar-vapor generator. *Adv. Funct. Mater.* **30**, 2003862 (2020).
135. Kim, I. et al. Ultrafast metaphotonic PCR chip with near-perfect absorber. *Adv. Mater.* **36**, 2311931 (2024).
136. Kumari, A., Yadav, A., Singh, O. P. & Sharan, P. A review of surface plasmon resonance (SPR) technology in biosensing: innovations, applications and future trends. *J. Opt*. https://doi.org/10.1007/s12596-024-02265-3 (2024).
137. Bakhtiar, R. Surface plasmon resonance spectroscopy: a versatile technique in a Biochemist's Toolbox. *J. Chem. Educ.* **90**, 203–209 (2013).
138. Singh, G. P. & Sardana, N. Smartphone-based surface plasmon resonance sensors: a review. *Plasmonics* **17**, 1869–1888 (2022).
139. Janith, G. I. et al. Advances in surface plasmon resonance biosensors for medical diagnostics: an overview of recent developments and techniques. *J. Pharm. Biomed. Anal. Open* **2**, 100019 (2023).
140. Shrivastav, A. M., Cvelbar, U. & Abdulhalim, I. A comprehensive review on plasmonic-based biosensors used in viral diagnostics. *Commun. Biol.* **4**, 70 (2021).
141. Yano, T. et al. Ultrasensitive detection of SARS-CoV-2 nucleocapsid protein using large gold nanoparticle-enhanced surface plasmon resonance. *Sci. Rep.* **12**, 1060 (2022).
142. Terao, K. et al. Fast protein detection in raw blood by size-exclusion SPR sensing. *Anal. Methods* **7**, 6483–6488 (2015).
143. Mondal, H. S., Ahmed, K. A., Birbilis, N. & Hossain, M. Z. Machine learning for detecting DNA attachment on SPR biosensor. *Sci. Rep.* **13**, 3742 (2023).
144. Neettiyath, A., Chung, K., Liu, W. & Lee, L. P. Nanoplasmonic sensors for extracellular vesicles and bacterial membrane vesicles. *Nano Converg.* **11**, 23 (2024).
145. Damborský, P., Švitel, J. & Katrlík, J. Optical biosensors. *Essays Biochem.* **60**, 91–100 (2016).
146. Svirelis, J., Andersson, J., Stradner, A. & Dahlin, A. Accurate correction of the "Bulk Response" in surface plasmon resonance sensing provides new insights on interactions involving lysozyme and poly(ethylene glycol). *ACS Sens.* **7**, 1175–1182 (2022).
147. Engheta, N., Salandrino, A. & Alù, A. Circuit elements at optical frequencies: nanoinductors, nanocapacitors, and nanoresistors. *Phys. Rev. Lett.* **95**, 95504 (2005).
148. Bhalla, N. & Shen, A. Q. Localized surface plasmon resonance sensing and its interplay with fluidics. *Langmuir* **40**, 9842–9854 (2024).
149. Xu, T. & Geng, Z. Strategies to improve performances of LSPR biosensing: structure, materials, and interface modification. *Biosens. Bioelectron.* **174**, 112850 (2021).
150. Hong, Y. A. & Ha, J. W. Enhanced refractive index sensitivity of localized surface plasmon resonance inflection points in single hollow gold nanospheres with inner cavity. *Sci. Rep.* **12**, 6983 (2022).
151. Park, J.-H., Byun, J.-Y., Shim, W.-B., Kim, S. U. & Kim, M.-G. High-sensitivity detection of ATP using a localized surface plasmon resonance (LSPR) sensor and split aptamers. *Biosens. Bioelectron.* **73**, 26–31 (2015).
152. Funari, R., Chu, K.-Y. & Shen, A. Q. Detection of antibodies against SARS-CoV-2 spike protein by gold nanospikes in an opto-microfluidic chip. *Biosens. Bioelectron.* **169**, 112578 (2020).
153. Kim, L. et al. Recombinant protein embedded liposome on gold nanoparticle based on LSPR method to detect Corona virus. *Nano Converg.* **10**, 51 (2023).
154. Waitkus, J. et al. Gold nanoparticle enabled localized surface plasmon resonance on unique gold nanomushroom structures for on-chip CRISPR-Cas13a sensing. *Adv. Mater. Interfaces* **10**, 2201261 (2023).
155. Im, H. et al. Label-free detection and molecular profiling of exosomes with a nano-plasmonic sensor. *Nat. Biotechnol.* **32**, 490–495 (2014).
156. Pang, R. et al. Development of a gold-nanorod-based lateral flow immunoassay for a fast and dual-modal detection of C-reactive protein in clinical plasma samples. *RSC Adv.* **11**, 28388–28394 (2021).
157. Yin, X. et al. Performance enhancement of the lateral flow immunoassay by use of composite nanoparticles as signal labels. *TrAC Trends Anal. Chem.* **170**, 117441 (2024).
158. Kakkar, S. et al. Lateral flow assays: progress and evolution of recent trends in point-of-care applications. *Mater. Today Bio* **28**, 101188 (2024).
159. Wu, Y. et al. Surface-enhanced raman scattering-based lateral flow assay strips using highly symmetric gold nanostars. *ACS Appl. Nano Mater.* **7**, 27134–27141 (2024).
160. Albrecht, M. G. & Creighton, J. A. Anomalously intense Raman spectra of pyridine at a silver electrode. *J. Am. Chem. Soc.* **99**, 5215–5217 (1977).
161. Jeanmaire, D. L. & Van Duyne, R. P. Surface Raman spectroelectrochemistry: Part I. Heterocyclic, aromatic, and aliphatic amines adsorbed on the anodized silver electrode. *J. Electroanal. Chem. Interfacial Electrochem.* **84**, 1–20 (1977).
162. Xu, H., Aizpurua, J., Käll, M. & Apell, P. Electromagnetic contributions to single-molecule sensitivity in surface-enhanced Raman scattering. *Phys. Rev. E* **62**, 4318–4324 (2000).
163. Sharma, B., Frontiera, R. R., Henry, A.-I., Ringe, E. & Van Duyne, R. P. SERS: materials, applications, and the future. *Mater. Today* **15**, 16–25 (2012).
164. Langer, J. et al. Present and future of surface-enhanced Raman scattering. *ACS Nano* **14**, 28–117 (2020).
165. Hang, Y., Boryczka, J. & Wu, N. Visible-light and near-infrared fluorescence and surface-enhanced Raman scattering point-of-care sensing and bio-imaging: a review. *Chem. Soc. Rev.* **51**, 329–375 (2022).
166. Ding, S.-Y. et al. Nanostructure-based plasmon-enhanced Raman spectroscopy for surface analysis of materials. *Nat. Rev. Mater.* **1**, 16021 (2016).
167. Kennedy, B. J., Spaeth, S., Dickey, M. & Carron, K. T. Determination of the distance dependence and experimental effects for modified sers substrates based on self-assembled monolayers formed using alkanethiols. *J. Phys. Chem. B* **103**, 3640–3646 (1999).
168. Han, X. X., Rodriguez, R. S., Haynes, C. L., Ozaki, Y. & Zhao, B. Surface-enhanced Raman spectroscopy. *Nat. Rev. Methods Prim.* **1**, 87 (2022).
169. Kleinman, S. L., Frontiera, R. R., Henry, A.-I., Dieringer, J. A. & Van Duyne, R. P. Creating, characterizing, and controlling chemistry with SERS hot spots. *Phys. Chem. Chem. Phys.* **15**, 21–36 (2013).

170. Stiles, L. P., Dieringer, A. J., Shah, C. N. & Van Duyne, P. R. Surface-enhanced Raman spectroscopy. *Annu. Rev. Anal. Chem.* **1**, 601–606 (2008).
171. Rodríguez-Lorenzo, L. et al. Zeptomol detection through controlled ultrasensitive surface-enhanced Raman scattering. *J. Am. Chem. Soc.* **131**, 4616–4618 (2009).
172. Chen, K. et al. Highly ordered Ag/Cu hybrid nanostructure arrays for ultrasensitive surface-enhanced Raman spectroscopy. *Adv. Mater. Interfaces* **3**, 1600115 (2016).
173. Li, X., Ren, X., Zhang, Y., Choy, W. C. H. & Wei, B. An all-copper plasmonic sandwich system obtained through directly depositing copper NPs on a CVD grown graphene/copper film and its application in SERS. *Nanoscale* **7**, 11291–11299 (2015).
174. Li, J. et al. A digital single-molecule nanopillar SERS platform for predicting and monitoring immune toxicities in immunotherapy. *Nat. Commun.* **12**, 1087 (2021).
175. Shin, H. et al. Single test-based diagnosis of multiple cancer types using exosome-SERS-AI for early stage cancers. *Nat. Commun.* **14**, 1644 (2023).
176. La, J. A., Lee, H., Kim, D., Ko, H. & Kang, T. Enhanced molecular interaction of 3D plasmonic nanoporous gold alloys by electronic modulation for sensitive molecular detection. *Nano Lett.* **24**, 7025–7032 (2024).
177. Kang, B., Austin, L. A. & El-Sayed, M. A. Observing real-time molecular event dynamics of apoptosis in living cancer cells using nuclear-targeted plasmonically enhanced Raman nanoprobes. *ACS Nano* **8**, 4883–4892 (2014).
178. Kang, B., Austin, L. A. & El-Sayed, M. A. Real-time molecular imaging throughout the entire cell cycle by targeted plasmonic-enhanced Rayleigh/Raman spectroscopy. *Nano Lett.* **12**, 5369–5375 (2012).
179. Nam, J.-M., Oh, J.-W., Lee, H. & Suh, Y. D. Plasmonic nanogap-enhanced Raman scattering with nanoparticles. *Acc. Chem. Res* **49**, 2746–2755 (2016).
180. Klaine, S. J. et al. Nanomaterials in the environment: behavior, fate, bioavailability, and effects. *Environ. Toxicol. Chem.* **27**, 1825–1851 (2008).
181. Yi, J. et al. Surface-enhanced Raman spectroscopy: a half-century historical perspective. *Chem. Soc. Rev.* **54**, 1453–1551 (2025).
182. Lin, C. et al. Recent development of surface-enhanced Raman scattering for biosensing. *J. Nanobiotechnol.* **21**, 149 (2023).
183. Chang, H., Hur, W., Kang, H. & Jun, B.-H. In vivo surface-enhanced Raman scattering techniques: nanoprobes, instrumentation, and applications. *Light Sci. Appl.* **14**, 79 (2025).
184. Quarin, S. M., Vang, D., Dima, R. I., Stan, G. & Strobbia, P. AI in SERS sensing moving from discriminative to generative. *npj Biosensing* **2**, 9 (2025).
185. de Albuquerque, C. D. L., Sobral-Filho, R. G., Poppi, R. J. & Brolo, A. G. Digital protocol for chemical analysis at ultralow concentrations by surface-enhanced Raman scattering. *Anal. Chem.* **90**, 1248–1254 (2018).
186. Kinkhabwala, A. et al. Large single-molecule fluorescence enhancements produced by a bowtie nanoantenna. *Nat. Photonics* **3**, 654–657 (2009).
187. Punj, D. et al. A plasmonic 'antenna-in-box' platform for enhanced single-molecule analysis at micromolar concentrations. *Nat. Nanotechnol.* **8**, 512–516 (2013).
188. Russell, K. J., Liu, T.-L., Cui, S. & Hu, E. L. Large spontaneous emission enhancement in plasmonic nanocavities. *Nat. Photonics* **6**, 459–462 (2012).
189. Ganesh, N. et al. Enhanced fluorescence emission from quantum dots on a photonic crystal surface. *Nat. Nanotechnol.* **2**, 515–520 (2007).
190. Rissin, D. M. et al. Single-molecule enzyme-linked immunosorbent assay detects serum proteins at subfemtomolar concentrations. *Nat. Biotechnol.* **28**, 595–599 (2010).
191. Liebermann, T. & Knoll, W. Surface-plasmon field-enhanced fluorescence spectroscopy. *Colloids Surf. A Physicochem. Eng. Asp.* **171**, 115–130 (2000).
192. Cheng, Z., Li, G. & Liu, M. Metal-enhanced fluorescence effect of Ag and Au nanoparticles modified with rhodamine derivative in detecting Hg2+. *Sens Actuators B Chem.* **212**, 495–504 (2015).
193. Su, Q., Jiang, C., Gou, D. & Long, Y. Surface plasmon-assisted fluorescence enhancing and quenching: from theory to application. *ACS Appl Bio Mater.* **4**, 4684–4705 (2021).
194. Li, J.-F., Li, C.-Y. & Aroca, R. F. Plasmon-enhanced fluorescence spectroscopy. *Chem. Soc. Rev.* **46**, 3962–3979 (2017).
195. Akselrod, G. M. et al. Probing the mechanisms of large Purcell enhancement in plasmonic nanoantennas. *Nat. Photonics* **8**, 835–840 (2014).
196. Xiong, Y. et al. Photonic crystal enhanced fluorescence emission and blinking suppression for single quantum dot digital resolution biosensing. *Nat. Commun.* **13**, 4647 (2022).
197. Luan, J. et al. Ultrabright fluorescent nanoscale labels for the femtomolar detection of analytes with standard bioassays. *Nat. Biomed. Eng.* **4**, 518–530 (2020).
198. Li, X. et al. Autoantibody profiling on a plasmonic nano-gold chip for the early detection of hypertensive. *Proc. Natl Acad. Sci. USA* **114**, 7089–7094 (2017).
199. Zhang, B., Kumar, R. B., Dai, H. & Feldman, B. J. A plasmonic chip for biomarker discovery and diagnosis of type 1 diabetes. *Nat. Med.* **20**, 948–953 (2014).
200. Gupta, R. et al. Ultrasensitive lateral-flow assays via plasmonically active antibody-conjugated fluorescent nanoparticles. *Nat. Biomed. Eng.* **7**, 1556–1570 (2023).
201. Liu, Y. et al. Multiplexed discrimination of SARS-CoV-2 variants via plasmonic-enhanced fluorescence in a portable and automated device. *Nat. Biomed. Eng.* **7**, 1636–1648 (2023).
202. Tabakman, S. M. et al. Plasmonic substrates for multiplexed protein microarrays with femtomolar sensitivity and broad dynamic range. *Nat. Commun.* **2**, 466 (2011).
203. Cheng, Y. et al. Fluorescence near gold nanoparticles for DNA sensing. *Anal. Chem.* **83**, 1307–1314 (2011).
204. Peng, M., Sun, F., Na, N. & Ouyang, J. Target-triggered assembly of nanogap antennas to enhance the fluorescence of single molecules and their application in MicroRNA detection. *Small* **16**, 2000460 (2020).
205. Mei, Z. & Tang, L. Surface-plasmon-coupled fluorescence enhancement based on ordered gold nanorod array biochip for ultrasensitive DNA analysis. *Anal. Chem.* **89**, 633–639 (2017).
206. Nooteboom, S. W. et al. Rate-engineered plasmon-enhanced fluorescence for real-time microsecond dynamics of single biomolecules. *Nano Lett.* **24**, 11641–11647 (2024).
207. Choi, S. & Nam, Y. S. Plasmon-modulated fluorescence nanoprobes for enzyme-free DNA detection via target signal enhancement and off-target quenching. *Biosens. Bioelectron.* **210**, 114288 (2022).
208. Braun, G. B. et al. Etchable plasmonic nanoparticle probes to image and quantify cellular internalization. *Nat. Mater.* **13**, 904–911 (2014).
209. Jeong, Y., Kook, Y.-M., Lee, K. & Koh, W.-G. Metal enhanced fluorescence (MEF) for biosensors: general approaches and a review of recent developments. *Biosens. Bioelectron.* **111**, 102–116 (2018).
210. Gan, W. et al. Atomically thin boron nitride as an ideal spacer for metal-enhanced fluorescence. *ACS Nano* **13**, 12184–12191 (2019).
211. Luan, J. et al. Add-on plasmonic patch as a universal fluorescence enhancer. *Light Sci. Appl.* **7**, 29 (2018).
212. Wang, M., Wang, M., Zheng, G., Dai, Z. & Ma, Y. Recent progress in sensing application of metal nanoarchitecture-enhanced fluorescence. *Nanoscale Adv.* **3**, 2448–2465 (2021).
213. Hou, S. et al. A self-assembled plasmonic substrate for enhanced fluorescence resonance energy transfer. *Adv. Mater.* **32**, 1906475 (2020).

214. Lee, K., Cui, Y., Lee, L. P. & Irudayaraj, J. Quantitative imaging of single mRNA splice variants in living cells. *Nat. Nanotechnol.* **9**, 474–480 (2014).
215. Yguerabide, J. & Yguerabide, E. E. Light-scattering submicroscopic particles as highly fluorescent analogs and their use as tracer labels in clinical and biological applications: II. Experimental characterization. *Anal. Biochem* **262**, 157–176 (1998).
216. Sönnichsen, C., Reinhard, B. M., Liphardt, J. & Alivisatos, A. P. A molecular ruler based on plasmon coupling of single gold and silver nanoparticles. *Nat. Biotechnol.* **23**, 741–745 (2005).
217. Mirkin, C. A., Letsinger, R. L., Mucic, R. C. & Storhoff, J. J. A DNA-based method for rationally assembling nanoparticles into macroscopic materials. *Nature* **382**, 607–609 (1996).
218. Elghanian, R., Storhoff, J. J., Mucic, R. C., Letsinger, R. L. & Mirkin, C. A. Selective colorimetric detection of polynucleotides based on the distance-dependent optical properties of gold nanoparticles. *Science ((1979))* **277**, 1078–1081 (1997).
219. Yoon, S. Controlled assembly of gold nanoparticles: methods and plasmon coupling properties. *Bull. Korean Chem. Soc.* **45**, 689–698 (2024).
220. Esteban, R., Borisov, A. G., Nordlander, P. & Aizpurua, J. Bridging quantum and classical plasmonics with a quantum-corrected model. *Nat. Commun.* **3**, 825 (2012).
221. Li, W. Physics models of plasmonics: single nanoparticle, complex single nanoparticle, nanodimer, and single nanoparticle over metallic thin film. *Plasmonics* **13**, 997–1014 (2018).
222. Zohar, N., Chuntonov, L. & Haran, G. The simplest plasmonic molecules: metal nanoparticle dimers and trimers. *J. Photochem. Photobiol. C***21**, 26–39 (2014).
223. Raschke, G. et al. Biomolecular recognition based on single gold nanoparticle light scattering. *Nano Lett.* **3**, 935–938 (2003).
224. Kim, E., Baaske, M. D., Schuldes, I., Wilsch, P. S. & Vollmer, F. Label-free optical detection of single enzyme-reactant reactions and associated conformational changes. *Sci. Adv.* **3**, e1603044 (2017).
225. Liu, G. L. Plasmon resonance energy transfer nanospectroscopy. in *Encyclopedia of Nanotechnology* (ed Bhushan, B.) 3264–3277 (Springer Netherlands, Dordrecht, 2016).
226. Ding, H., Lin, X. & Liu, X. Investigation on how spectral overlap between donor–acceptor affects PRET. *Appl. Phys. A* **127**, 917 (2021).
227. Kim, I. et al. Metasurfaces-driven hyperspectral imaging via multiplexed plasmonic resonance energy transfer. *Adv. Mater.* **35**, 2300229 (2023).
228. Neubrech, F. et al. Resonant plasmonic and vibrational coupling in a tailored nanoantenna for infrared detection. *Phys. Rev. Lett.* **101**, 157403 (2008).
229. Liu, G. L., Doll, J. C. & Lee, L. P. High-speed multispectral imaging of nanoplasmonic array. *Opt. Express* **13**, 8520–8525 (2005).
230. Choi, Y., Park, Y., Kang, T. & Lee, L. P. Selective and sensitive detection of metal ions by plasmonic resonance energy transfer-based nanospectroscopy. *Nat. Nanotechnol.* **4**, 742–746 (2009).
231. Choi, Y., Kang, T. & Lee, L. P. Plasmon resonance energy transfer (PRET)-based molecular imaging of cytochrome C in living cells. *Nano Lett.* **9**, 85–90 (2009).
232. Cao, Y., Xie, T., Qian, R. C. & Long, Y. T. Plasmon resonance energy transfer: coupling between chromophore molecules and metallic nanoparticles. *Small* **13**, 1601955 (2017).
233. Hong, S. G., Lee, M. Y., Jackson, A. O. & Lee, L. P. Bioinspired optical antennas: gold plant viruses. *Light Sci. Appl.* **4**, e267 (2015).
234. Jain, A. et al. Wireless electrical–molecular quantum signalling for cancer cell apoptosis. *Nat. Nanotechnol.* **19**, 106–114 (2024).
235. Kwon, J. A. et al. Tunable plasmonic cavity for label-free detection of small molecules. *ACS Appl. Mater. Interfaces* **10**, 13226–13235 (2018).
236. Lee, J. Y. et al. Real-time investigation of cytochrome c release profiles in living neuronal cells undergoing amyloid beta oligomer-induced apoptosis. *Nanoscale* **7**, 10340–10343 (2015).
237. Land, K. J., Boeras, D. I., Chen, X.-S., Ramsay, A. R. & Peeling, R. W. REASSURED diagnostics to inform disease control strategies, strengthen health systems and improve patient outcomes. *Nat. Microbiol.* **4**, 46–54 (2019).
238. Network, T. D. D. for A. The potential of digital molecular diagnostics for infectious diseases in sub-Saharan. *Afr. PLOS Digit. Health* **1**, e0000064 (2022).
239. Lee, S. et al. Sample-to-answer platform for the clinical evaluation of COVID-19 using a deep learning-assisted smartphone-based assay. *Nat. Commun.* **14**, 2361 (2023).
240. Lee, S. et al. Rapid deep learning-assisted predictive diagnostics for point-of-care testing. *Nat. Commun.* **15**, 1695 (2024).
241. Han, G.-R. et al. Machine learning in point-of-care testing: innovations, challenges, and opportunities. *Nat. Commun.* **16**, 3165 (2025).
242. Zhu, C. S. et al. Identification of procathepsin L (pCTS-L)–neutralizing monoclonal antibodies to treat potentially lethal sepsis. *Sci. Adv.* **9**, eadf4313 (2025).
243. Hargreaves, M. Handheld Raman, SERS, and SORS. in *Portable Spectroscopy and Spectrometry* (eds R. Crocombe, P. Leary & B. Kammrath) 347–376 (2021).
244. Sachdeva, S., Davis, R. W. & Saha, A. K. Microfluidic point-of-care testing: commercial landscape and future directions. *Front. Bioeng. Biotechnol.* **8**, 602659 (2021).
245. Schasfoort, R. B. M. & McWhirter, A. SPR Instrumentation. in *Handbook of Surface Plasmon Res*onance (eds Kooyman, R. P. H. et al.) (The Royal Society of Chemistry, 2008).
246. Jason-Moller, L., Murphy, M. & Bruno, J. Overview of Biacore systems and their applications. *Curr. Protoc. Protein Sci.* **45**, 19.13.1–19.13.14 (2006).
247. Pappas H. & Frisch P. *Leveraging Technology as a Response to the COVID Pandemic*. (Productivity Press, 2022).
248. Knowling, S., Clark, J., Sjuts, H. & Abdiche, Y. Direct comparison of label-free biosensor binding kinetics obtained on the Biacore 8 K and the Carterra LSA. *SLAS Discov.***25**, 247255522093481 (2020).
249. Cetin, A. E. et al. Handheld high-throughput plasmonic biosensor using computational on-chip imaging. *Light Sci. Appl.* **3**, e122 (2014).
250. Boutal, H. et al. A multiplex lateral flow immunoassay for the rapid identification of NDM-, KPC-, IMP- and VIM-type and OXA-48-like carbapenemase-producing Enterobacteriaceae. *J. Antimicrob. Chemother.* **73**, 909–915 (2018).
251. U.S. Food and Drug Administration. *510(k) Substantial Equivalence Determination Decision Summary: NG-Test CARBA 5*. https://www.accessdata.fda.gov/cdrh_docs/reviews/K191889.pdf (2019).
252. European Commission. *NG-Test CARBA 5*. https://ec.europa.eu/tools/eudamed/#/screen/search-device/2714eed3-a427-4914-a037-727ee10a12b4 (2022).
253. Akalın, P. & Yazgan-Karataş, A. Development of a nucleic acid-based lateral flow device as a reliable diagnostic tool for respiratory viral infections. *MethodsX* **11**, 102372 (2023).
254. Hutagalung, S. V. et al. Development of nucleic acid lateral flow immunoassay for molecular detection of *Entamoeba moshkovskii* and *Entamoeba dispar* in stool samples. *Sci. Rep.* **14**, 6635 (2024).
255. Xu, K., Zhou, R., Takei, K. & Hong, M. Toward flexible surface-enhanced Raman scattering (SERS) sensors for point-of-care diagnostics. *Adv. Sci.* **6**, 1900925 (2019).
256. Tahir, M. A. et al. Klarite as a label-free SERS-based assay: a promising approach for atmospheric bioaerosol detection. *Analyst* **145**, 277–285 (2020).
257. Hankus, M. E., Stratis-Cullum, D. N. & Pellegrino, P. M. Surface enhanced Raman scattering (SERS)-based next generation commercially available substrate: physical characterization and biological application. in *Proc. SPIE* vol. 8099 80990N (2011).
258. Rahmani, M. et al. Highlight on commercial SERS substrates and on optimized nanorough large-area SERS-based sensors: a Raman study. *Appl. Nanosci.* **14**, 203–215 (2024).

259. Nanopartz Inc. Plasmonic PCR. https://www.nanopartz.com/plasmonic-pcr.asp?srsltid=AfmBOopwOHM9oc0ShFk9w4sFz0T0iCITjD7zyJZSOAD82ONwLEH3M6xG (2025).
260. Hayes, J. et al. Performance and functional assessment of the Kimera P-IV point-of-care plasmonic qPCR prototype for ultra rapid pathogen detection of chlamydia trachomatis. *Epidemiol. Infect.* **153**, e27 (2025).
261. Aksu, S. et al. High-throughput nanofabrication of infrared plasmonic nanoantenna arrays for vibrational nanospectroscopy. *Nano Lett.* **10**, 2511–2518 (2010).
262. Suresh, V., Ding, L., Chew, A. B. & Yap, F. L. Fabrication of large-area flexible SERS substrates by nanoimprint lithography. *ACS Appl. Nano Mater.* **1**, 886–893 (2018).
263. Oliverio, M., Perotto, S., Messina, G. C., Lovato, L. & De Angelis, F. Chemical functionalization of plasmonic surface biosensors: a tutorial review on issues, strategies, and costs. *ACS Appl. Mater. Interfaces* **9**, 29394–29411 (2017).
264. Hoang, T. et al. Room temperature roll-to-roll additive manufacturing of polydimethylsiloxane-based centrifugal microfluidic device for on-site isolation of ribonucleic acid from whole blood. *Mater. Today Bio* **23**, 100838 (2023).
265. Lopez, G. A., Estevez, M.-C., Soler, M. & Lechuga, L. M. Recent advances in nanoplasmonic biosensors: applications and lab-on-a-chip integration. *Nanophotonics* **6**, 123–136 (2017).
266. Escobedo, C. & Brolo, A. G. Synergizing microfluidics and plasmonics: advances, applications, and future directions. *Lab Chip* **25**, 1256–1281 (2025).
267. Dahlin, A. B., Wittenberg, N. J., Höök, F. & Oh, S.-H. Promises and challenges of nanoplasmonic devices for refractometric biosensing. *Nanophotonics* **2**, 83–101 (2013).
268. Lei, Z. & Guo, B. 2D material-based optical biosensor: status and prospect. *Adv. Sci.* **9**, 2102924 (2022).
269. Oh, S.-H. et al. Nanophotonic biosensors harnessing van der Waals materials. *Nat. Commun.* **12**, 3824 (2021).
270. Yadav, P. K. et al. 2D material–based surface plasmon resonance biosensors for applications in different domains: an insight. *Microchim. Acta* **191**, 373 (2024).
271. Hopper, E. R., Boukouvala, C., Asselin, J., Biggins, J. S. & Ringe, E. Opportunities and challenges for alternative nanoplasmonic metals: magnesium and beyond. *J. Phys. Chem. C***126**, 10630–10643 (2022).
272. Wang, Y. et al. Wearable plasmonic-metasurface sensor for noninvasive and universal molecular fingerprint detection on biointerfaces. *Sci. Adv.* **7**, eabe4553 (2021).
273. Cohen, M. et al. Wireless communication with nanoplasmonic data carriers: macroscale propagation of nanophotonic plasmon polaritons probed by near-field nanoimaging. *Nano Lett.* **17**, 5181–5186 (2017).
274. Kavungal, D. et al. Artificial intelligence–coupled plasmonic infrared sensor for detection of structural protein biomarkers in neurodegenerative diseases. *Sci. Adv.* **9**, eadg9644 (2023).
275. Chung, K. et al. Biological cavity quantum electrodynamics via self-aligned nanoring doublets: QED-SANDs. *J. Am. Chem. Soc.* **146**, 31150–31158 (2024).
276. Kokin, E. et al. Quantum electrodynamic behavior of chlorophyll in a plasmonic nanocavity. *Nano Lett.* **22**, 9861–9868 (2022).
277. Kim, H. et al. Ultrasensitive and real-time optical detection of cellular oxidative stress using graphene-covered tunable plasmonic interfaces. *Nano Converg.* **9**, 23 (2022).
278. Li, Z., Wang, P., Tong, L. & Zhang, L. Gold nanorod-facilitated localized heating of droplets in microfluidic chips. *Opt. Express* **21**, 1281–1286 (2013).
279. Son, J. H. et al. Ultrafast photonic PCR. *Light Sci. Appl.* **4**, e280 (2015).
280. Lee, J.-H. et al. Plasmonic photothermal gold bipyramid nanoreactors for ultrafast real-time bioassays. *J. Am. Chem. Soc.* **139**, 8054–8057 (2017).
281. Ye, H. et al. Plasmonic LAMP: improving the detection specificity and sensitivity for SARS-CoV-2 by plasmonic sensing of isothermally amplified nucleic acids. *Small* **18**, 2107832 (2022).
282. Seo, S. E. et al. Ultrafast molecular diagnosis-based solid-phase photonic PCR for respiratory pathogen variant discrimination. *Adv. Funct. Mater.* **34**, 2402972 (2024).
283. Kang, B.-H. et al. Ultrafast plasmonic nucleic acid amplification and real-time quantification for decentralized molecular diagnostics. *ACS Nano* **17**, 6507–6518 (2023).
284. Whang, K. et al. Capillarity-driven enrichment and hydrodynamic trapping of trace nucleic acids by plasmonic cavity membrane for rapid and sensitive detections. *Adv. Mater.* **36**, 2403896 (2024).
285. Whang, K. et al. Plasmonic bacteria on a nanoporous mirror via hydrodynamic trapping for rapid identification of waterborne pathogens. *Light Sci. Appl* **7**, 68 (2018).
286. Khandelwal, P., Singh, D. K. & Poddar, P. Advances in the experimental and theoretical understandings of antibiotic conjugated gold nanoparticles for antibacterial applications. *ChemistrySelect* **4**, 6719–6738 (2019).
287. McNay, G., Eustace, D., Smith, W. E., Faulds, K. & Graham, D. Surface-enhanced Raman scattering (SERS) and surface-enhanced resonance Raman scattering (SERRS): a review of applications. *Appl. Spectrosc.* **65**, 825–837 (2011).
288. Kelly, K. L., Coronado, E., Zhao, L. L. & Schatz, G. C. The optical properties of metal nanoparticles: the influence of size, shape, and dielectric environment. *J. Phys. Chem. B* **107**, 668–677 (2003).
289. Lyon, S. B. Corrosion of Noble Metals. in *Shreir's Corrosion* (eds Cottis, B. et al.) 2205–2223 (Elsevier, Oxford, 2010).
290. Huang, X. & El-Sayed, M. A. Gold nanoparticles: Optical properties and implementations in cancer diagnosis and photothermal therapy. *J. Adv. Res.* **1**, 13–28 (2010).
291. Xin, Y. et al. Copper-based plasmonic catalysis: recent advances and future perspectives. *Adv. Mater.* **33**, 2008145 (2021).
292. Knight, M. W. et al. Aluminum for plasmonics. *ACS Nano* **8**, 834–840 (2014).
293. Chung, K. et al. Non-oxidized bare copper nanoparticles with surface excess electrons in air. *Nat. Nanotechnol.* **17**, 285–291 (2022).
294. Dong, X. et al. Shape control of silver nanoparticles by stepwise citrate reduction. *J. Phys. Chem. C***113**, 6573–6576 (2009).
295. Agnihotri, S., Mukherji, S. & Mukherji, S. Size-controlled silver nanoparticles synthesized over the range 5-100 nm using the same protocol and their antibacterial efficacy. *RSC Adv.* **4**, 3974–3983 (2014).
296. Link, S. & El-Sayed, M. A. Size and temperature dependence of the plasmon absorption of colloidal gold nanoparticles. *J. Phys. Chem. B* **103**, 4212–4217 (1999).
297. Shafiqa, A. R., Abdul Aziz, A. & Mehrdel, B. Nanoparticle optical properties: size dependence of a single gold spherical nanoparticle. *J. Phys. Conf. Ser.* **1083**, 012040 (2018).
298. Luther, J. M., Jain, P. K., Ewers, T. & Alivisatos, A. P. Localized surface plasmon resonances arising from free carriers in doped quantum dots. *Nat. Mater.* **10**, 361–366 (2011).
299. Alvarez, M. M. et al. Optical absorption spectra of nanocrystal gold molecules. *J. Phys. Chem. B* **101**, 3706–3712 (1997).
300. Xu, D., Mao, J., He, Y. & Yeung, E. S. Size-tunable synthesis of high-quality gold nanorods under basic conditions by using H2O2 as the reducing agent. *J. Mater. Chem. C***2**, 4989–4996 (2014).
301. Rozenberg, M. et al. High yield seedless synthesis of mini gold nanorods: partial silver decoupling allows effective nanorod elongation with tunable surface plasmon resonance beyond 1000 nm and CTAB-free functional coating for mTHPC conjugation. *Nanoscale Adv.* **6**, 4831–4841 (2024).

302. González-Rubio, G. et al. Disconnecting symmetry breaking from seeded growth for the reproducible synthesis of high quality gold nanorods. *ACS Nano* **13**, 4424–4435 (2019).
303. Nassau, K. The Physics and Chemistry of Color: The 15 Mechanisms. *The Science of Color* (*Second Edition*) 7, 247–280 (2003).
304. Skrabalak, S. E. et al. Gold nanocages: synthesis, properties, and applications. *Acc. Chem. Res* **41**, 1587–1595 (2008).
305. Chen, X.-H., Zhu, J., Li, J.-J. & Zhao, J.-W. A plasmonic and SERS dual-mode iodide ions detecting probe based on the etching of Ag-coated tetrapod gold nanostars. *J. Nanopart. Res.* **21**, 158 (2019).
306. Bustamante, C. J., Chemla, Y. R., Liu, S. & Wang, M. D. Optical tweezers in single-molecule biophysics. *Nat. Rev. Methods Prim.* **1**, 25 (2021).
307. Draine, B. T. The discrete-dipole approximation and its application to interstellar graphite grains. *Astrophys. J.* **333**, 848 (1988).
308. Novotny, L., Bian, R. X. & Xie, X. S. Theory of nanometric optical tweezers. *Phys. Rev. Lett.* **79**, 645–648 (1997).
309. Yang, A. H. J., Lerdsuchatawanich, T. & Erickson, D. Forces and transport velocities for a particle in a slot waveguide. *Nano Lett.* **9**, 1182–1188 (2009).
310. Kolbow, J. D., Lindquist, N. C., Ertsgaard, C. T., Yoo, D. & Oh, S.-H. Nano-optical tweezers: methods and applications for trapping single molecules and nanoparticles. *ChemPhysChem* **22**, 1409–1420 (2021).
311. Seil, T. J. & Webster, J. T. Antimicrobial applications of nanotechnology: methods and literature. *Int. J. Nanomed.* **7**, 2767–2781 (2012).
312. Dexter, D. L. A theory of sensitized luminescence in solids. *J. Chem. Phys.* **21**, 836–850 (1953).
313. Lai, R. et al. Shallow distance-dependent triplet energy migration mediated by endothermic charge-transfer. *Nat. Commun.* **12**, 1532 (2021).
314. Chadwick, S. J., Salah, D., Livesey, P. M., Brust, M. & Volk, M. Singlet oxygen generation by laser irradiation of gold nanoparticles. *J. Phys. Chem. C* **120**, 10647–10657 (2016).
315. Kovalev, D. & Fujii, M. Silicon nanocrystals: photosensitizers for oxygen molecules. *Adv. Mater.* **17**, 2531–2544 (2005).
316. Fujii, M. et al. Chemical reaction mediated by excited states of Si nanocrystals—singlet oxygen formation in solution. *J. Appl. Phys.* **95**, 3689–3693 (2004).
317. Chakraborty, R. et al. A simple, fast and cost-effective method of synthesis of cupric oxide nanoparticle with promising antibacterial potency: Unraveling the biological and chemical modes of action. *Biochim. Biophys. Acta* **1850**, 845–856 (2015).
318. Sen, S. & Sarkar, K. Effective biocidal and wound healing cogency of biocompatible glutathione: citrate-capped copper oxide nanoparticles against multidrug-resistant pathogenic enterobacteria. *Microb. Drug Resist.* **27**, 616–627 (2021).
319. Brongersma, M. L., Halas, N. J. & Nordlander, P. Plasmon-induced hot carrier science and technology. *Nat. Nanotechnol.* **10**, 25–34 (2015).
320. Blicher, A., Wodzinska, K., Fidorra, M., Winterhalter, M. & Heimburg, T. The temperature dependence of lipid membrane permeability, its quantized nature, and the influence of anesthetics. *Biophys. J.* **96**, 4581–4591 (2009).
321. Kinnunen, P. K. J. On the principles of functional ordering in biological membranes. *Chem. Phys. Lipids* **57**, 375–399 (1991).
322. Chen, W., Duša, F., Witos, J., Ruokonen, S. K. & Wiedmer, S. K. Determination of the main phase transition temperature of phospholipids by nanoplasmonic sensing. *Sci. Rep.* **8**, 14815 (2018).
323. Xiong, R. et al. Photothermal nanomaterial-mediated photoporation. *Acc. Chem. Res* **56**, 631–643 (2023).
324. Palankar, R. et al. Nanoplasmonically-induced defects in lipid membrane monitored by ion current: Transient nanopores versus membrane rupture. *Nano Lett.* **14**, 4273–4279 (2014).
325. Chatterjee, D. K., Diagaradjane, P. & Krishnan, S. Nanoparticle-mediated hyperthermia in cancer therapy. *Ther. Deliv.* **2**, 1001–1014 (2011).
326. Prisner, L. et al. Monitoring the death of single BaF3 cells under plasmonic photothermal heating induced by ultrasmall gold nanorods. *J. Mater. Chem. B* **7**, 3582–3589 (2019).
327. Bartczak, D. et al. Interactions of human endothelial cells with gold nanoparticles of different morphologies. *Small* **8**, 122–130 (2012).
328. Zhao, X. et al. In situ single-cell surgery and intracellular organelle manipulation via thermoplasmonics combined optical trapping. *Nano Lett.* **22**, 402–410 (2022).
329. Yamanouchi K. *Quantum Mechanics of Molecular Structures*. (Springer Berlin, Heidelberg, 2012).
330. Clegg, R. M. 1.24 Fluorescence and FRET: Theoretical Concepts 101. in *Comprehensive Biophysics* (ed Egelman, E. H.) 592–617 (Elsevier, Amsterdam, 2012).
331. Zhu, W. et al. Quantum mechanical effects in plasmonic structures with subnanometre gaps. *Nat. Commun.* **7**, 11495 (2016).

Acknowledgements

This research was supported by the Air Force Office of Scientific Research Grants AFOSR FA2386-20-1-4060, NIH 5R01DK133864, NIH R01AG084098 and by the National Research Foundation of Korea (RS-20210NR061784). Cartoons in Boxes 1, 2a, b, 3b, c, 3e, f and Figs. 4, 5a, i were created with BioRender.com.

Author contributions

L.P.L. and K.C. supervised the study, reviewed, and edited the paper. H.T. wrote this review. T.H. wrote the discussion part and made substantial contributions to the discussions on all topics and edited the paper. All authors have read and approved the paper.

Competing interests

The authors declare no competing interests.

Additional information

Correspondence and requests for materials should be addressed to Kyungwha Chung or Luke P. Lee.